nagra.

Arbeitsbericht NAB 20-09

TBO Trüllikon-1-1: Data Report

Dossier VI
Wireline Logging and Micro-hydraulic Fracturing

June 2021

J. Gonus, E. Bailey, J. Desroches &
R. Garrard

National Cooperative
for the Disposal of
Radioactive Waste

Hardstrasse 73
P.O. Box 280
5430 Wettingen
Switzerland
Tel. +41 56 437 11 11

www.nagra.ch

nagra.

Arbeitsbericht NAB 20-09

TBO Trüllikon-1-1: Data Report

Dossier VI Wireline Logging and Micro-hydraulic Fracturing

June 2021

J. Gonus[1], E. Bailey[1], J. Desroches[1] & R. Garrard[2]

[1] GPCI Geneva Petroleum Consultants International
[2] Nagra

Keywords:
TRU1-1, Zürich Nordost, TBO, deep drilling campaign, wireline logging, petrophysical logging, in situ testing, micro-hydraulic fracturing

National Cooperative for the Disposal of Radioactive Waste

Hardstrasse 73
P.O. Box 280
5430 Wettingen
Switzerland
Tel. +41 56 437 11 11

www.nagra.ch

Nagra Arbeitsberichte ("Working Reports") present the results of work in progress that have not necessarily been subject to a comprehensive review. They are intended to provide rapid dissemination of current information.

This NAB aims at reporting drilling results at an early stage. Additional borehole-specific data will be published elsewhere.

In the event of inconsistencies between dossiers of this NAB, the dossier addressing the specific topic takes priority. In the event of discrepancies between Nagra reports, the chronologically later report is generally considered to be correct. Data sets and interpretations laid out in this NAB may be revised in subsequent reports. The reasoning leading to these revisions will be detailed there.

This Dossier was prepared by a project team consisting of:
J. Gonus (petrophysics QC, theoretical concepts, log analysis)
E. Bailey (introductory chapters, BHI QC, project management)
J. Desroches (MHF QC, theoretical concepts) and
R. Garrard (coordination, QC review)

Editorial work: Graphics and editing teams at Nagra

Petrophysical log graphic files were created using Geolog Emerson E&P Software - Emerson Paradigm and Terrastation.

The Dossier has greatly benefitted from reviews by external and internal experts. Their input and work are very much appreciated.

Table of Contents

List of Tables

List of Figures

List of Appendices

Note: Only in the digital version of this report Appendices A – E can be found under the paper clip symbol.

1 Introduction

1.1 Context

To provide input for site selection and the safety case for deep geological repositories for radioactive waste, Nagra has drilled a series of deep boreholes in Northern Switzerland. The aim of the drilling campaign is to characterise the deep underground of the three remaining siting regions located at the edge of the Northern Alpine Molasse Basin (Fig. 1-1).

In this report, we present the results from the Trüllikon-1-1 borehole.

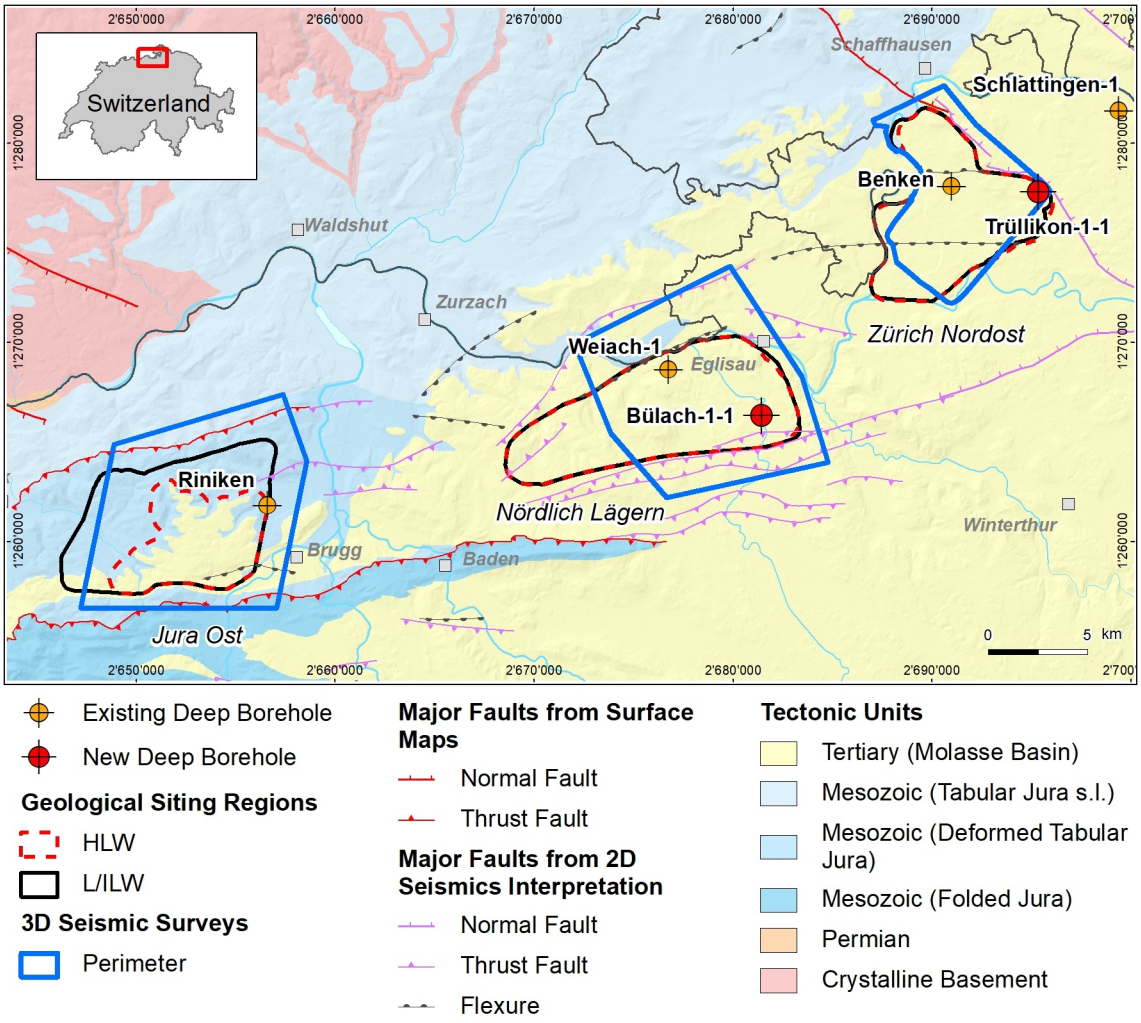

Fig. 1-1: Tectonic overview map with the three siting regions under investigation

1.2 Location and specifications of the borehole

The Trüllikon-1-1 (TRU1-1) exploratory borehole is the second borehole drilled within the framework of the TBO project. The drill site is located in the eastern part of the Zürich Nordost siting region (Fig. 1-2). The vertical borehole reached a final depth of 1'310 m (MD)[1]. The borehole specifications are provided in Tab. 1-1.

Tab. 1-1: General information about the TRU1-1 borehole

Siting region	Zürich Nordost
Municipality	Trüllikon (Canton Zürich / ZH), Switzerland
Drill site	Trüllikon-1 (TRU1)
Borehole	Trüllikon-1-1 (TRU1-1)
Coordinates	LV95: 2'695'372.648 / 1'277'548.076
Elevation	Ground level = top of rig cellar: 475.07 m above sea level (asl)
Borehole depth	1'310.0 m measured depth (MD) below ground level (bgl)
Drilling period	15. August 2019 – 5. April 2020 (spud date to end of rig release)
Drilling company	PR Marriott Drilling Ltd.
Drilling rig	Rig-16 Drillmec HH102
Drilling fluid	Water-based mud with various amounts of different components such as[2]: 46 – 712 m: Pure-Bore® 712 – 1'161 m: Potassium silicate 1'161 – 1'310 m: Sodium chloride & polymers

The lithostratigraphic profile and the casing scheme are shown in Fig. 1-3. The comparison of the core versus log depth[3] of the main lithostratigraphic boundaries in the TRU1-1 borehole is shown in Tab. 1-2.

[1] Measured depth (MD) refers to the position along the borehole trajectory, starting at ground level, which for this borehole is the top of the rig cellar. For a perfectly vertical borehole, MD below ground level (bgl) and true vertical depth (TVD) are the same. In all Dossiers depth refers to MD unless stated otherwise.

[2] For detailed information see Dossier I.

[3] Core depth refers to the depth marked on the drill cores. Log depth results from the depth observed during geophysical wireline logging. Note that the petrophysical logs have not been shifted to core depth, hence log depth differs from core depth.

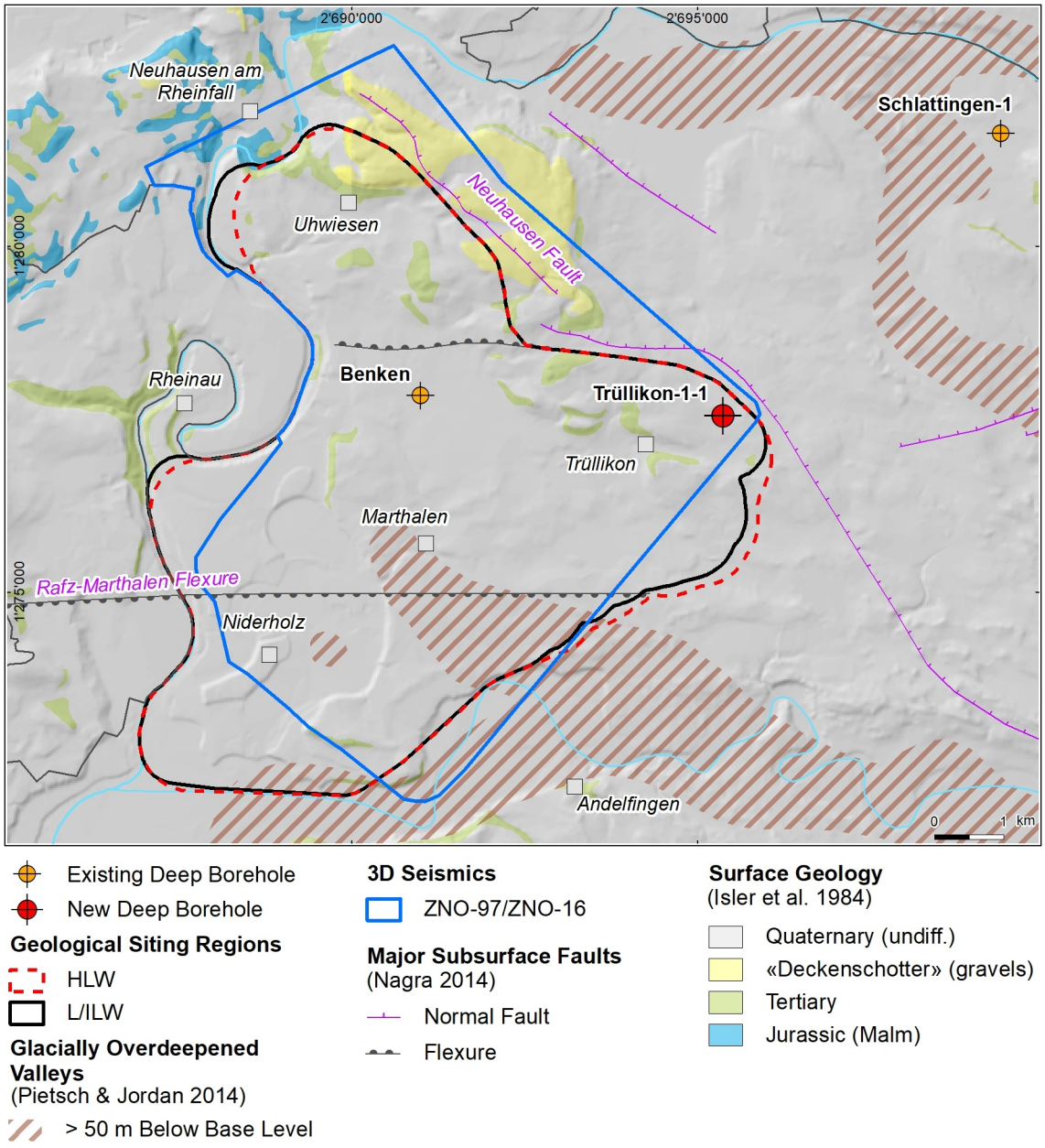

Fig. 1-2: Overview map of the investigation area in the Zürich Nordost siting region with the location of the TRU1-1 borehole in relation to the boreholes Benken and Schlattingen

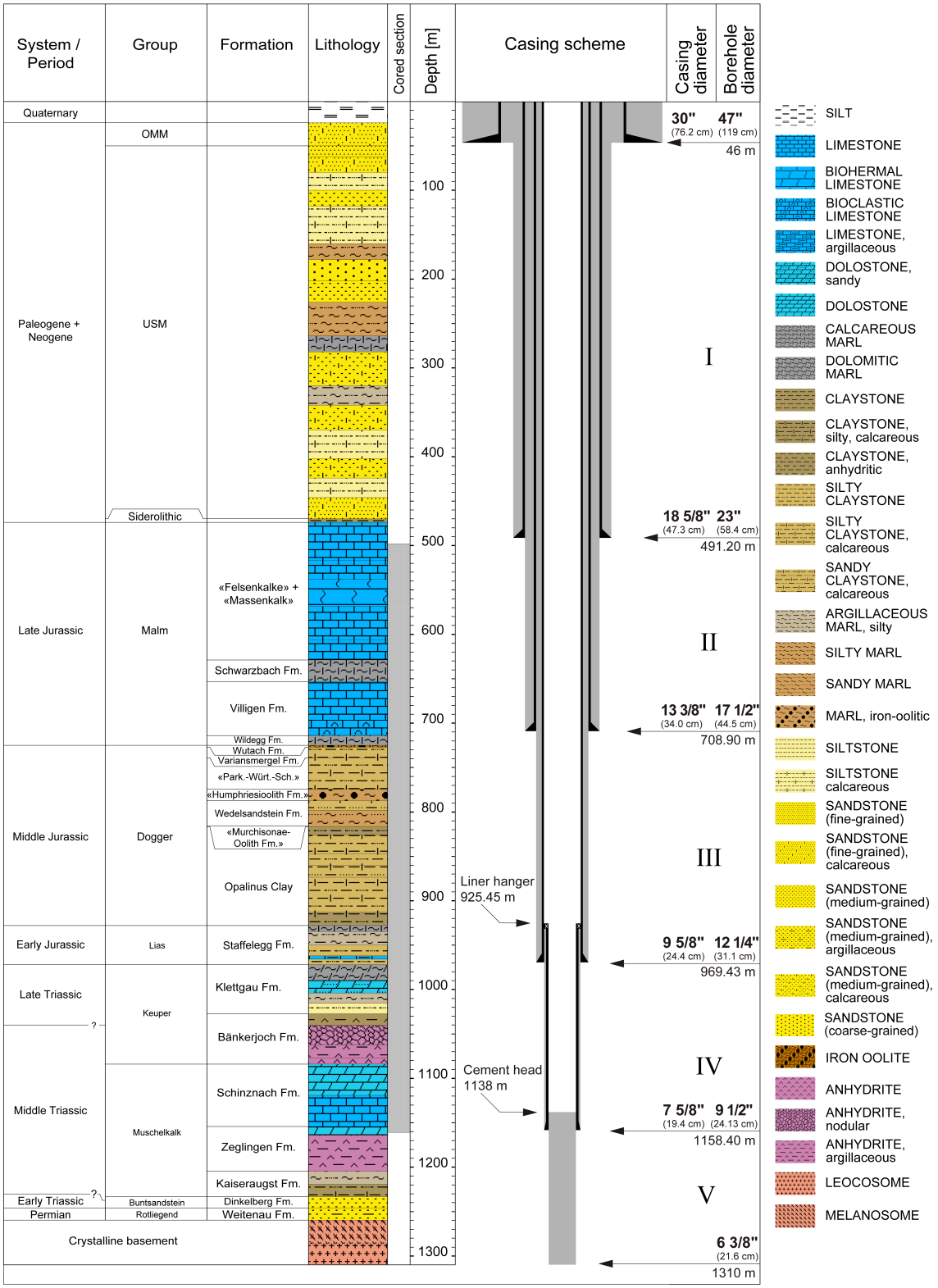

Fig. 1-3: Lithostratigraphic profile and casing scheme for the TRU1-1 borehole[4]

[4] For detailed information see Dossier I and III.

Tab. 1-2: Core and log depth for the main lithostratigraphic boundaries in the TRU1-1 borehole[5]

System / Period	Group	Formation	Core depth in m (MD)	Log depth in m (MD)	
Quaternary				**24.0**	—
Paleogene + Neogene	OMM			50.0	—
	USM			470.0	—
	Siderolithic			**474.0**	—
Jurassic	Malm	«Felsenkalke» + «Massenkalk»	628.87	628.75	—
		Schwarzbach Formation	653.29	653.15	—
		Villigen Formation	714.00	714.00	—
		Wildegg Formation	724.85	725.03	—
	Dogger	Wutach Formation	727.13	727.27	—
		Variansmergel Formation	738.97	739.06	—
		«Parkinsoni-Württembergica-Schichten»	774.55	774.66	—
		«Humphriesioolith Formation»	787.50	787.55	—
		Wedelsandstein Formation	815.51	815.50	—
		«Murchisonae-Oolith Formation»	816.42	816.43	—
		Opalinus Clay	927.91	927.87	—
	Lias	Staffelegg Formation	**971.68**	**971.55**	—
Triassic	Keuper	Klettgau Formation	1027.22	1027.44	—
		Bänkerjoch Formation	1084.01	1084.22	—
	Muschelkalk	Schinznach Formation	1154.25	1154.43	—
		Zeglingen Formation	1204.5		—
		Kaiseraugst Formation	1233.2		—
	Buntsandstein	Dinkelberg Formation	**1246.1**		—
Permian	Rotliegend	Weitenau Formation	**1259.7**		—
		Crystalline Basement	1310.0	final depth	

[5] For details regarding lithostratigraphic boundaries see Dossier III; for details about depth shifts (core goniometry) see Dossier V.

1.3 Documentation structure for the TRU1-1 borehole

NAB 20-09 documents the majority of the investigations carried out in the TRU1-1 borehole, including laboratory investigations on core material. The NAB comprises a series of stand-alone dossiers addressing individual topics and a final dossier with a summary composite plot (Tab. 1-3).

This documentation aims at early publication of the data collected in the TRU1-1 borehole. It includes most of the data available approximately one year after completion of the borehole. Some analyses are still ongoing (e.g. diffusion experiments, analysis of veins, hydrochemical interpretation of water samples) and results will be published in separate reports.

The current borehole report will provide an important basis for the integration of datasets from different boreholes. The integration and interpretation of the results in the wider geological context will be documented later in separate geoscientific reports.

Tab. 1-3: List of dossiers included in NAB 20-09

Black indicates the dossier at hand.

Dossier	Title	Authors
I	TBO Trüllikon-1-1: Drilling	M. Ammen & P.-J. Palten
II	TBO Trüllikon-1-1: Core Photography	D. Kaehr & M. Gysi
III	TBO Trüllikon-1-1: Lithostratigraphy	M. Schwarz, P. Jordan, P. Schürch, H. Naef, T. Ibele, R. Felber & M. Gysi
IV	TBO Trüllikon-1-1: Microfacies, Bio- and Chemostratigraphic Analyses	S. Wohlwend, H.R. Bläsi, S. Feist-Burkhardt, B. Hostettler, U. Menkveld-Gfeller, V. Dietze & G. Deplazes
V	TBO Trüllikon-1-1: Structural Geology	A. Ebert, S. Cioldi, L. Gregorczyk, S. Rust, D. Böhni & M. Gysi
VI	TBO Trüllikon-1-1: Wireline Logging and Microhydraulic Fracturing	J. Gonus, E. Bailey, J. Desroches & R. Garrard
VII	TBO Trüllikon-1-1: Hydraulic Packer Testing	R. Schwarz, L. Schlickenrieder, H.R. Müller, S. Köhler, A. Pechstein & T. Vogt
VIII	TBO Trüllikon-1-1: Rock Properties, Porewater Characterisation and Natural Tracer Profiles	L. Aschwanden, L. Camesi, T. Gimmi, A. Jenni, M. Kiczka, U. Mäder, M. Mazurek, D. Rufer, H.N. Waber, P. Wersin, C. Zwahlen & D. Traber
IX	TBO Trüllikon-1-1: Rock-mechanical and Geomechanical Laboratory Testing	E. Crisci, L. Laloui & S. Giger
X	TBO Trüllikon-1-1: Petrophysical Log Analysis	S. Marnat & J.K. Becker
	TBO Trüllikon-1-1: Summary Plot	Nagra

1.4 Scope and objectives of this dossier

This dossier describes the acquisition, quality control and results of the Petrophysical Logging (PL) and Microhydraulic Fracturing (MHF) wireline logging measurements performed in the TRU1-1 borehole.

Petrophysical log measurements were acquired in open borehole conditions (no casing) with wireline conveyed logging tools to determine continuous profiles across the borehole of physical and chemical properties of the formation, including its mineralogy, clay types, porosity, fluid content, and acoustic properties. Petrophysical logs were further acquired to obtain high-resolution circumferential images of the borehole wall, as well as to measure borehole physical parameters such as its geometry, mud resistivity and mud temperature. In addition to the open hole logs, temperature logs were acquired post completion to measure the undisturbed mud temperature.

A series of in-situ stress measurements were performed using the microhydraulic fracturing technique to estimate the orientation and magnitude of the earth stress at different depths. The objectives of the MHF testing program were to provide estimates of the in-situ stress state in the Opalinus Clay potential rock host and adjacent rock formations and provide calibration points for mechanical earth models (MEM) of the rock mass (1D, 3D).

All PL and MHF testing were performed by the wireline logging company Schlumberger (SLB). Geneva Petroleum Consultants International (GPCI) were responsible for planning wireline operations, technical supervision at the worksite, quality assurance and control (QA-QC) of data, database management and general wireline logging support.

This dossier is organised as follows:

- Chapter 2: The sequence of events for PL and MHF testing operations, and associated log / data coverage is provided.
- Chapter 3: The QA-QC procedure used to assess the quality of the petrophysical logs is detailed. A continuous profile of each log across the entire measured depth of the borehole is quality-controlled, corrected and spliced together to generate a quality-controlled composite log. The results of the composite log are discussed. The composite log will then be used as the final log data for input into further data analysis processes such as formation evaluation (e.g. Stochastic Petrophysical Log Analysis described in Dossier X), calibration with seismic data, and integration with sedimentology and structural geology data (from cores, cuttings, adjacent boreholes, and regional geology).
- Chapter 4: Although Borehole Imagery (BHI) logs were acquired as a part of petrophysical logging, the objectives of BHI are related to both Structural Geology (analysis of image features described in Dossier V) and MHF (firstly the selection of stations for MHF stress measurements, then the analysis of fractures induced by MHF tests). Thus, the QC, processing and interpretation processes of BHI are described in a chapter separate from the QA-QC procedures of the other petrophysical logs in Chapter 3.
- Chapter 5: MHF test procedures and preliminary results are presented.
- Finally, this report includes a set of appendices, where spliced PL, pre- and post-MHF borehole images and MHF data can be found.

2 Wireline logging and testing operations

The Trüllikon-1-1 (TRU1-1) borehole was planned in 5 drilling sections (also commonly referred to as phases). After installation of the 30" outer diameter (OD) standpipe, Section I was drilled and logged in the 23" drill bit size. Sections II through V were continuously cored using the 6⅜" core bit and subsequently logged / tested. After wireline logging operations in each section were completed, the borehole was reamed (opened up) to 17½" (Section II), 12¼" (Section III) and 9½" (Section IV) to accommodate the OD 13⅜" casing, 9⅝" casing and 7⅝" liner, respectively. Once open borehole logging / testing operations were completed, the borehole was backfilled with cement up to 1'138 m MD (inside the 9⅝" OD casing). One post-completion, petrophysical log was acquired to measure the undisturbed mud temperature. Detailed descriptions of the borehole design and mud conditions at the time of logging and testing are included in the excel Composite Report (Appendix A), under the worksheets entitled 'Borehole design' and 'Hole & mud system'. Additional details about borehole configuration, casing and cementing scheme and mud parameters can be found in Dossier I.

Wireline logging and testing operations were divided into the following groups of activities:

- Petrophysical Logging (PL)
- Microhydraulic Fracturing (MHF)
- *Technical Logging (TL)*
- *Vertical Seismic Profiling (VSP)*

Petrophysical logs are continuous measurements (recorded every half foot or approximately 15 cm) of mineralogy and physical properties of formation rocks, their contained fluids, and the borehole environment between the wireline conveyed logging tool sensors and the borehole wall. Petrophysical logs were acquired with conventional and advanced wireline-conveyed logging tools. Conventional tools measured Depth (measured depth [MD], or log depth, that is the depth reference for all wireline measurements), Total Gamma Ray (naturally occurring gamma radiation), Spontaneous Potential (electric potential difference between the formation and an electrode at surface), Temperature, Caliper (measurement of the borehole diameter), Inclinometer (measurement of the borehole trajectory), as well as the standard "quad combo" tools: Resistivity (electrical resistivity at different depths of investigation in the formation), Sonic (compressional and shear wave slowness), Density (measurement of the bulk density and the photoelectric factor), and Neutron (measurement of the neutron hydrogen index, a proxy of porosity, as well as the sigma capture cross-section). Advanced tools measured the Spectral Gamma Ray (potassium, thorium and uranium contributions to the total naturally occurring gamma radiation), Elemental Spectroscopy, and Microresistivity and Ultrasonic borehole images. These logging tools and their main measurements are described in detail in the subsequent Chapter 3 – Petrophysical Logging and Chapter 4 – Borehole Imagery.

MHF involves using wireline-conveyed testing equipment to initiate and analyse the characteristics of microhydraulic fractures through several opening / closure cycles, to estimate the current stress state in the rock formation at the 1 m scale. Tests were conducted using the SLB Modular Formation Dynamics Tester (MDT), which uses packer modules, surface-controlled valves, pressure gauges and a downhole pump to initiate and propagate fractures at predefined discrete depths. MHF tests are described in Chapter 5 – Microhydraulic Fracturing.

As well as PL and MHF operations, wireline operations also included Technical Logging (TL) and Vertical Seismic Profiling (VSP). TL acquired data on the physical properties of the open borehole (geometry and trajectory) and the permanent casing installation. The borehole geometry

was measured using calipers for both assessing the borehole condition (breakouts / washouts present) and determining the volume of cement needed for casing installations. The borehole inclination and azimuth were measured to confirm the borehole verticality and identify its trajectory. To assess the quality of the cement behind the casing, Cement Bond Logs (CBL) were acquired using a sonic tool. Borehole deviation surveys, cement volume calculations and CBL logs are described in Dossier I. VSP acquired high resolution borehole seismic measurements used for correlation with, and enhancement of, surface seismic data. VSP will be addressed in a separate document. TL and VSP are not described further in this report.

A summary of all wireline logging and testing activities carried out in the TRU1-1 borehole is given in Tab. 2-1. Fig. 2-1 depicts graphically the log coverage for the PL and MHF testing campaigns. In total, 5 PL and 4 MHF testing campaigns were undertaken. Open hole PL was conducted in all sections of TRU1-1, whilst MHF testing was conducted in Sections II to V. A more detailed analysis of the log measurement coverage is provided in Chapter 3.

Details of the logging runs, logging dates, wireline logging company, logging interval, logging suite and principal measurements acquired for PL and MHF operations are provided in Tab. 2-2. Mnemonics for each tool in the logging suite listed in this table are given in Tab. 2-3.

Tab. 2-1: Logging and testing activities during drilling of the TRU1-1 borehole

Drilling phase / section	**Borehole diameter and section TD**	**Permanent casing size** **Casing / liner shoe depth**	**Start date**	**End date**	**Coring**	**Technical logging**	**Petrophysical logging**	**Microhydraulic fracturing**	**Vertical seismic profiling**
I	23" to 493.0 m	18⅝" 0 to 491.20 m	15.08.2019	13.09.2019		×	×		
II	17½" to 710.65 m 12¼" to 710.70 m 6⅜" to 712 m	13⅜" 0 to 708.90 m	13.09.2019	18.11.1019	×	×	×	×	×
III	12¼" to 971.85 m 8½" to 973 m	9⅝" 0 to 969.43 m	18.11.1019	26.01.2020	×	×	×	×	
IV	9½" to 1'159.76 m 8½" to 1'161 m	7⅝" 925.45 to 1'158.40 m	26.01.2020	20.03.2020	×	×	×	×	
V	6⅜" to 1'310 m	n/a	20.03.2020	03.04.2020	×		×	×	×

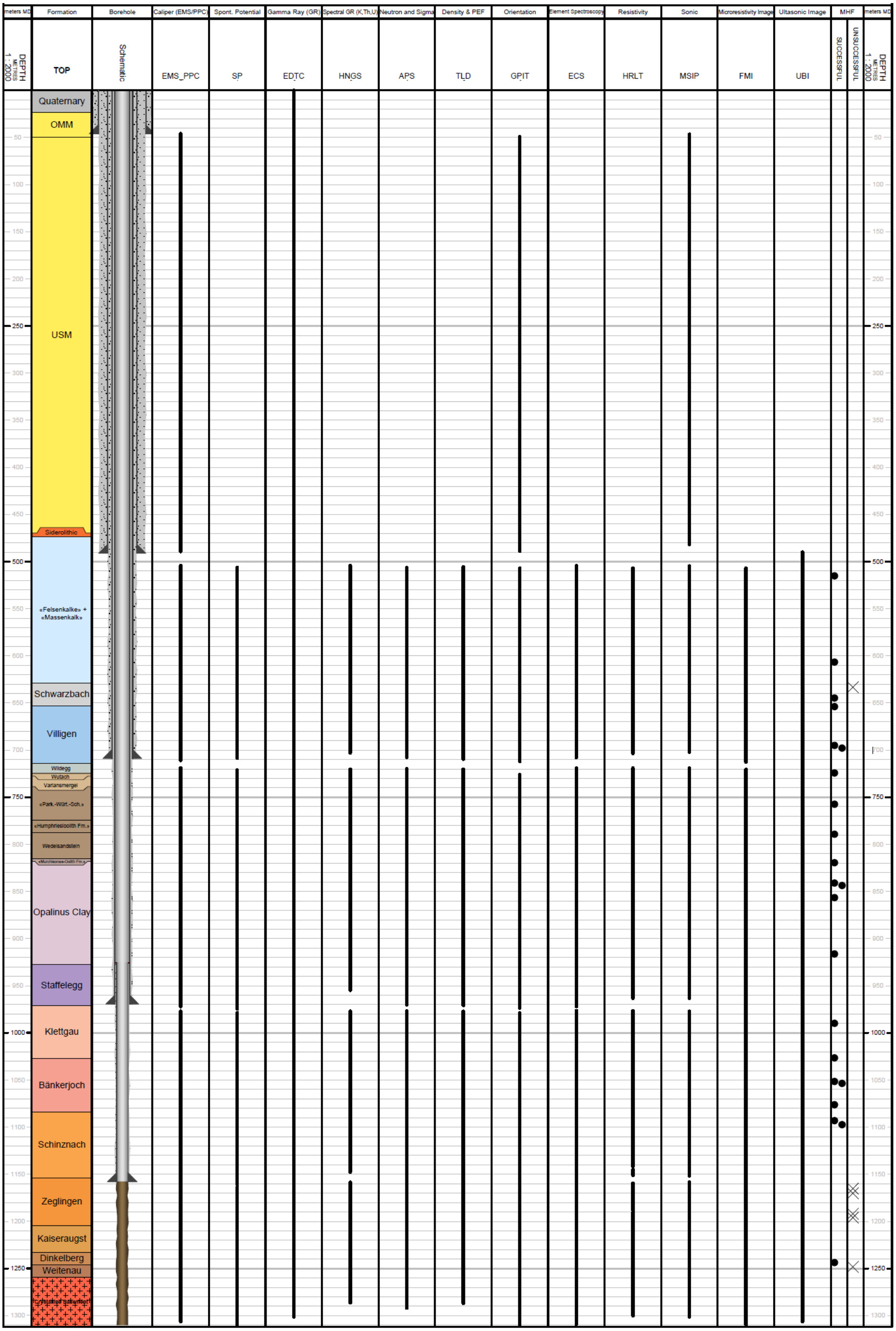

Fig. 2-1: Petrophysical log and MHF testing coverage at TRU1-1 (scale of 1:2'000)

Tab. 2-2: Logging and testing sequence of events (only PP L and MHF)

Phase / Section	**Run**	**Operation**	**Logging date**	**Contractor**	**Logging interval** [m MD]	**Logging suite** (see list of abbreviations)	**Measurements**																**Remarks**
							Gamma ray	**Resistivity**	**Microresistivity**	**Density**	**Sonic**	**Neutron hydrogen index**	**Sigma capture cross-section**	**Photoelectric factor**	**Spontaneous potential**	**Borehole imaging**	**Caliper**	**Spectral gamma ray**	**Elemental spectroscopy**	**Inclinometer**	**Temperature**	**MHF**	
I	1.1.1	PL	01.09.2019	SLB	495.6 to 21.2	GPIT-PPC-MSIP-PPC-EMS-EDTC-LEH.QT	×				×						×			×	×		Poor quality Sonic, Density and PEF data (large hole). Only Sonic is of good quality below Molasse / Malm interface
	1.1.2		01.09.2019	SLB	491.95 to 36.1	TLD-MCFL-EDTC-LEH.QT	×		×	×				×									
II	2.1.1	PL	08.10.2019	SLB	712.6 to 512.2	FMI-EMS-EDTC-LEH.QT	×									×	×			×	×		
	2.1.2		08.10.2019	SLB	710.9 to 490	UBI-GPIT-EMS-PPC-EDTC-LEH.QT	×									×	×			×	×		
	2.1.3		08.10.2019	SLB	710.8 to 490.1	PPC-MSIP-PPC-GPIT-EMS-EDTC-LEH.QT	×				×						×			×	×		
	2.1.4		08. – 09.10.2019	SLB	712.4 to 490.1	SP-PPC-HRLT- EMS-EDTC-LEH.QT	×	×							×		×				×		
	2.1.5		09.10.2019	SLB	708.3 to 490.1	APS-EMS-EDTC-LEH.QT	×					×	×				×				×		
	2.1.6		09.10.2019	SLB	710.9 to 490	TLD-MCFL-EMS-EDTC-LEH.QT	×		×	×							×				×		
	2.1.7		09.10.2019	SLB	710.3 to 490.1	ECS-HNGS-EMS-EDTC-LEH.QT	×										×	×	×		×		
	2.1.8	MHF	09. – 11.10.2019	SLB	7 stations	MRPA-(straddle)-MRPA(single)-MRSC(exit)-MRPS-MRHY-MRSCx4-MRSC(exit)-EDTC-LEH.QT																×	6 successful tests out of 7
	2.1.9	PL	11. – 12.10.2019	SLB	711.1 to 506.8	FMI-EMS-EDTC-LEH.QT	×									×	×			×	×		Post-MHF
	2.1.10	MDT Sampling	12. – 13.10.2019	SLB	Fluid sampling	MRPA-(straddle)-MRPA(single)-MRSC(exit)-MRPS-MRHY-MRSCx4-MRSC(exit)-EDTC-LEH.QT	×															×	3 samples recovered

Tab. 2-2: continued

Phase / Section	Run	Operation	Logging date	Contractor	Logging interval [m MD]	Logging suite (see list of abbreviations)	Measurements																Remarks
							Gamma ray	Resistivity	Microresistivity	Density	Sonic	Neutron hydrogen index	Sigma capture cross-section	Photoelectric factor	Spontaneous potential	Borehole imaging	Caliper	Spectral gamma ray	Elemental spectroscopy	Inclinometer	Temperature	MHF	
III	3.1.1	PL	25. – 26.11.2019	SLB	822.3 to 720.6	FMI-EMS-EDTC-LEH.QT	×									×	×			×	×		
	3.3.1	PL	18.12.2019	SLB	974.3 to 780	FMI-EMS-EDTC-LEH.QT	×									×	×			×	×		
	3.4.1	PL	24.12.2019	SLB	972.4 to 675.1	EMS-EDTC-LEH.QT	×										×				×		
	3.4.2		24.12.2019	SLB	971.1 to 695.4	UBI-GPIT-EMS-EDTC-LEH.QT	×									×	×				×		
	3.4.3	MHF	24. – 26.12.2019	SLB	8 stations	MRPA(straddle)-MRPA(single)-MRSC(exit)-MRPO(HP)-5xMRSC(water)-MRSC(exit)-EDTC-LEH.QT	×															×	8 successful tests out of 8
	3.4.4	PL	26.10.2019	SLB	973 to 703	FMI-EMS-EDTC-LEH.QT (post-MHF)	×									×	×			×	×		Post-MHF
	3.4.5		26. – 27.12.2019	SLB	972.6 to 676.8	PPC-MSIP-PPC-GPIT-EMS-EDTC-LEH.QT	×				×						×			×	×		
	3.4.6		27.12.2019	SLB	974.6 to 697.8	SP-EMS-HRLT-EDTC-LEH.QT	×	×									×				×		
	3.4.7		27.12.2019	SLB	970 to 693.8	APS-EMS-EDTC-LEH.QT	×					×	×				×				×		
	3.4.8		27.12.2019	SLB	971.2 to 694.7	TLD-MCFL-EMS-EDTC-LEH.QT	×		×	×				×			×				×		
	3.4.9		27.12.2019	SLB	972 to 678	ECS-HNGS -EMS-EDTC-LEH.QT	×										×	×	×		×		
IV	4.2.1	PL	19.02.2020	SLB	1'157.6 to 903.1	PPC-MSIP-PPC-GPIT-EMS-EDTC-LEH.QT	×				×						×			×	×		
	4.2.2		19.02.2020	SLB	1'158.7 to 968.6	FMI-EDTC-LEH.QT	×									×	×			×			
	4.2.3		20.02.2020	SLB	1'157.3 to 963	APS-EMS-EDTC-LEH.QT	×					×	×				×				×		
	4.2.4		20.02.2020	SLB	1'089.4 to 970	TLD-MCFL-EDTC-LEH.QT	×		×	×				×									Tool string hung up at 1'045 m; uplog from this depth
	4.2.5		20.02.2020	SLB	1'161.7 to 960.1	SP-EMS-HRLT-EDTC-LEH.QT	×	×							×		×				×		

Tab. 2-2: continued

Phase / Section	Run	Operation	Logging date	Contractor	Logging interval [m MD]	Logging suite (see list of abbreviations)	Measurements																Remarks
							Gamma ray	Resistivity	Microresistivity	Density	Sonic	Neutron hydrogen index	Sigma capture cross-section	Photoelectric factor	Spontaneous potential	Borehole imaging	Caliper	Spectral gamma ray	Elemental spectroscopy	Inclinometer	Temperature	MHF	
IV continued	4.2.6	PL	20.02.2020	SLB	1'161.1 to 970	TLD-MCFL-EDTC-LEH.QT	×		×	×				×									TLD re-run to obtain data over the entire open hole section
	4.2.7		20. – 21.02.2020	SLB	1'159.3 to 950.4	ECS-HNGS-EDTC-LEH.QT	×											×	×				
	4.3.1	PL	26.02.2020	SLB	1'160.8 to 947.3	EMS-EDTC-LEH.QT	×										×				×		
	4.3.2		26.02.2020	SLB	1'156.7 to 960	UBI-GPIT-EMS-EDTC-LEH.QT	×									×	×			×	×		
	4.4.1	PL	02.03.2020	SLB	1'125.7 to 960.9	FMI-EMS-EDTC-LEH.QT	×									×	×			×	×		Borehole was enlarged to 8½" down to 1'122 m after it degraded in the 6⅜" section
	4.4.2	MHF	02. – 04.03.2020	SLB	3 stations	MRPA(straddle)-MRPA(single)-MRSC(exit)-MRPO(hp)-5xMRSC(water)-MRSC(exit)-EDTC-LEH.QT	×															×	3 successful tests out of 3. Run aborted due to tool failure and poor borehole conditions; wiper trip performed
	4.5.1	PL	05.03.2020	SLB	1'124.9 to 960.1	EMS-EDTC-LEH.QT	×										×				×		
	4.5.2	MHF	05. – 06.03.2020	SLB	4 stations	MRPA(straddle)-MRPA(single)-MRSC(exit)-MRPO(hp)-5xMRSC(water)-MRSC(exit)-EDTC-LEH.QT	×															×	4 successful tests out of 4
	4.5.3	PL	06.03.2020	SLB	1'121.9 to 968.2	FMI-EMS-EDTC-LEH.QT	×									×	×			×	×		Post-MHF run

Tab. 2-2: continued

Phase / Section	Run	Operation	Logging date	Contractor	Logging interval [m MD]	Logging suite (see list of abbreviations)	Measurements																Remarks
							Gamma ray	Resistivity	Microresistivity	Density	Sonic	Neutron hydrogen index	Sigma capture cross-section	Photoelectric factor	Spontaneous potential	Borehole imaging	Caliper	Spectral gamma ray	Elemental spectroscopy	Inclinometer	Temperature	MHF	
V	5.1.1	PL	28. – 29.03.2020	SLB	1'131.3 to 1'148.5	FMI-EMS-EDTC-LEH.QT	×									×	×			×	×		
	5.1.3		30. – 31.03.2020	SLB	1'306.2 to 1'153.5	UBI-GPIT-EMS-EDTC-LEH.QT	×									×	×			×	×		
	5.1.4		31.03.2020	SLB	1'309.7 to 1'138.9	PPC-MSIP-PPC-GPIT-EDTC-LEH.QT	×				×						×			×			
	5.1.5		31.03.2020	SLB	1'309.1 to 1'142.8	ECS-HNGS-EDTC-LEH.QT	×											×	×				
	5.1.6		31.03.2020	SLB	1'131.7 to 1'143.8	SP-EMS-HRLT-APS-TLD-MCFL-EDTC-LEH.QT	×	×	×	×		×	×	×	×		×				×		
	5.1.7	MHF	31.03. – 02.04.2020	SLB	6 stations	MRPA(straddle)-MRPA(single)-MRSC(exit)-MRPO(hp)-4xMRSC(water)-MRSC(exit)-EDTC-LEH.QT	×															×	1 successful test out of 6
	5.1.8	PL	02.04.2020	SLB	1'309.7 to 1'152.4	FMI-EMS-EDTC-LEH.QT	×									×	×			×	×		Post-MHF
	5.2.1	PL	09.04.2021	SLB	0 to 1'132.8	EMS-EDTC-LEH.QT	×														×		Post-completion

Tab. 2-3: Tool mnemonics and measurement details

Logging tool	**Wireline contractor**	**Mnemonic**	**Principal measurement**
APS	SLB	Accelerator porosity sonde	Epithermal and thermal neutrons, sigma capture cross-section of thermal neutrons
ASLT	SLB	Array sonic logging tool	For cement evaluation / cement bond log (CBL)
ECS	SLB	Elemental capture spectroscopy sonde	Measurement of the relative dry weight element concentration (e.g. Si, Ca, Fe, S, Ti, Gd, Cl and H) and mineralogical model
EDTC	SLB	Enhanced digital telemetry cartridge	Gamma ray measurement of the total natural radioactivity
EMS	SLB	Environmental measurement sonde	6-arm caliper, temperature and mud resistivity
FMI	SLB	Fullbore formation microimager	Microresistivity imaging tool (pad contact)
GPIT	SLB	General purpose inclinometry tool	Orientation/inclination of the borehole
HNGS	SLB	Hostile natural gamma ray sonde	Spectral gamma ray measurements of natural radioactivity (potassium, thorium, uranium)
HRLT	SLB	High resolution laterolog array tool	Laterolog resistivity measurement at different depths of investigation
IBC	SLB	Isolation Scanner (IBCS-D sub)	Ultrasonic and flexural wave imaging
LEH.QT	SLB	Logging equipment head with tension	Head tension
MCFL	SLB	Microcylindrically focused log	Measures the invaded zone resistivity (Rxo)
MRHY	SLB	Optical Fluid Analyzer	Measures the composition of the flowing fluid (mud, water)
MRPA	SLB	Packer modules	Packer modules for MHF tests
MRPO	SLB	Pump out module	Downhole pump for MHF tests
MRPS	SLB	Probe module	Single point formation pressure / mobility measurement
MRSC	SLB	Sample chamber	Carrying fluid for MHF tests, filled with water, sometimes air for special tests. Also used as a receptacle for fluid sampling.
MSIP	SLB	Modular sonic imaging platform (sonic scanner)	Compressional, shear and Stoneley wave slowness measurements (monopole and dipole sources); cement bond log
PPC	SLB	Power positioning calipers	4-arm caliper that gives dual axis borehole measurements

Tab. 2-3: continued

Logging tool	**Wireline contractor**	**Mnemonic**	**Principal measurement**
SP	SLB	Spontaneous potential	Measurement of electrical potential difference between the borehole and the surface
TLD	SLB	Three-detector lithology density	Bulk density and photoelectric absorption factor measurement
UBI	SLB	Ultrasonic borehole imager	High-resolution acoustic (ultrasonic) images of the borehole
USIT	SLB	Ultrasonic imaging tool	360° ultrasonic radial cement image for assessing cement coverage in the annulus and identifying channels

3 Petrophysical Logging (PL)

3.1 Petrophysical logging tools and measurements

Below the main petrophysical measurements acquired, and the downhole logging tools deployed are summarised. A detailed description of how the different tools measure the respective parameters and the underlying physics behind these measurements is not the focus of this report. Borehole imaging tools are described in Chapter 4.

- **Borehole deviation / orientation** (GPIT – General Purpose Inclinometry Tool). The GPIT outputs inclinometer measurements. Tool orientation is defined by three parameters: tool deviation, tool azimuth and relative bearing. Borehole trajectory is calculated from the inclinometer measurements. Inclinometer measurements serve to reference the oriented logs (e.g. borehole imagery and sonic dipole logs).
- **Caliper log** (EMS/PPC – Environmental Measurement Sonde/Powered Positioning Caliper). The caliper log uses several coupled pairs of mechanical arms (2 pairs with PPC, 3 pairs with EMS) to continuously measure the borehole shape in different orientations.
- **Density** (TLD – Three-detector Lithology Density). TLD is an induced radiation tool that measures the bulk density of the formation and the photoelectric factor (PEF). It uses a radioactive source to emit gamma photons into the formation. The gamma rays undergo Compton scattering by interacting with the atomic electrons in the formation. Compton scattering reduces the energy of the gamma rays in a stepwise manner and scatters the gamma rays in all directions. When the energy of the gamma rays is less than 0.5 MeV, they can undergo photoelectric absorption by interacting with the atomic electrons. The flux of gamma rays that reach each of the detectors of the TLD is therefore attenuated by the formation, and the amount of attenuation is dependent upon the density of electrons in the formation, which is related to its bulk density. The bulk density of a rock is the sum of the minerals (solids) and fluids volumes (porosity) times their densities. Hence, the formation density tool is key for the determination of porosity, the detection of low-density fluids (gasses) in the pores and lithological identification. In addition, the TLD provides the **photoelectric absorption index** (photoelectric factor – PEF), which represents the probability that a gamma photon will be photo-electrically absorbed per electron of the atoms that compose the material. The PEF characterises the mineralogy. The TLD tool is housed in the High-Resolution Mechanical Sonde that also includes the Micro-Cylindrically Focused Log (MCFL) sonde, that measures the **microresistivity** or alternatively, the resistivity very close to the borehole wall (RXOZ). The bulk density was integrated over depth, to provide the overburden pressure or vertical stress (Sv).
- **Element Spectroscopy** (ECS – Elemental Capture Spectroscopy). The ECS is also an induced radiation tool with a radioactive neutron source. The ECS measures the concentration of a series of elements in the formation (Si, Ca, Fe, S, Ti, Gd, Cl, H) by analysing the gamma ray spectrum of back scattered gamma rays. Special processing techniques allow under certain circumstances the measurement of supplementary elements such as Al, Mg, K and Na. The element spectroscopy measurements are provided in dry weight elements. SLB uses an algorithm in the field to derive a model of dry weight fractions of minerals from the dry weight element concentrations: clay, clastics (quartz – feldspar – mica, QFM), carbonates, anhydrite / gypsum, salt / evaporite, pyrite and siderite. Advanced models can discriminate limestone and dolomite from carbonates, as well to provide a more quantitative clay measurement. It is important to note that mineralogy model processing is qualitative and should be viewed as an indicator of lithology and not used in any quantitative analysis. Quantitative analysis of the ECS dry weight elements needs to be calibrated against core data. Dossier X

details stochastic processing and interpretation of the ECS dry weight proportions, combined with conventional petrophysical log response, to generate a quantified lithology determination.

- **Gamma Ray** (GR, from the EDTC – Enhanced Digital Telemetry Cartridge). This log measures the total naturally occurring gamma ray radioactivity in the formation rocks (potassium, thorium and uranium are the most common radioactive elements in Earth's crust), which can be used to determine the volume of clay minerals (that contains those elements). The GR log is not valid for clay determination if other minerals contain those elements in significant amounts (e.g. potassic feldspars, organic matter, phosphates). The GR is run with all logging runs because it is used for depth correlation between runs, thanks to its excellent vertical resolution and character. Note this is not to be confused with the Spectral Gamma Ray which is a different tool detailed further below.
- **Neutron Hydrogen Index, commonly named Neutron** (NHI, from the APS – Accelerator Porosity Sonde). A particular accelerator called a Minitron generates high energy neutrons (14 MeV) that are emitted into the formation. Elastic collisions with the atom nuclei slow down the neutrons, a process that is more efficient with nuclei whose mass is close to that of neutron, i.e., hydrogen (the lightest element). Five detectors count the neutrons back from the formation at different distances from the Minitron, allowing for an environmental compensation of the signal. The received signal is mostly (but not only, for example the carbon atoms bring a significant contribution) dependent on the hydrogen concentration in the formation, hence the Hydrogen Index (HI) measurement: the larger the count, the lower the HI and its uncertainty. The APS tool can measure both an epithermal HI (APLC curve) and a thermal HI (FPLC). The hydrogen content in rocks is mostly in the fluids contained within, generally water or hydrocarbons, which have a HI close to 1 v/v. Nevertheless, some fluids like gas and high salinity brines have a HI lower than 1 v/v and must be corrected for when interpreting the results. In addition, many hydrated minerals are encountered in sedimentary or crystalline rocks, e.g. clay minerals, gypsum, iron-hydroxides, coals, zeolites, micas and amphiboles. The NHI is commonly used to quantify the fluid volume (porosity) and as a lithological indicator (clay content, hydrogen-rich minerals), mostly in combination with the bulk density measurement.
- **Resistivity** (HRLT – High Resolution Laterolog array Tool). The HRLT measures electrical resistivities at different depths of investigation in the formation. When drilling mud filtrate invades the formation and it has a salinity that contrasts with that of the formation fluids (the chlorine ion Cl^- changes significantly the resistivity of a medium), the resistivities provide an invasion profile. Processing allows the extrapolation of the resistivity measurements far into the formation providing the true formation resistivity, as well as close to the tool providing the microresistivity or resistivity close to the borehole wall. Resistivity is used to interpret the saturation in water or hydrocarbons in pore spaces.
- **Sigma Formation Capture Cross-Section** (SIGF, from APS). In addition to the HI, the APS also measures the sigma formation capture cross-section (SIGF), that is defined as the relative ability of a material to "capture" or absorb free thermal neutrons. SIGF values vary widely with elements, and it can be used to determine the mineralogy and formation fluid contents.
- **Sonic** (MSIP – Modular Sonic Imaging Platform, also named Sonic Scanner). The MSIP measures how fast compressional and shear waves travel in the formation. A pulse sound is emitted from several tool transmitters in all directions. Tool receivers record the waves after they have travelled through a known path in the formation to the borehole wall. Waves travel at different velocities in the drilling fluid (between the tool and the borehole wall) and in the formation. Subtracting the travel time recorded by the near transmitter-receiver pairs from the travel time recorded by far transmitter-receiver pairs provides the travel time spent in the

formation only and thus discards the wave propagation in the fluid. Travel times are converted to wave slowness logs (inverse of velocity) based on the tool geometry. Compressional and shear wave slowness are used to interpret porosity, aid in mineralogy determination, for geomechanical and rock strength properties and they serve as calibration for seismic surveys. Other wave propagation modes are also recorded by the MSIP (oriented shear waves, Rayleigh waves, Stoneley waves). Oriented shear waves can be used to analyse the acoustic anisotropy properties of the formation. The MSIP log products require processing of the raw data to detect the different wave arrivals and transform the multiple transmitter-receiver recordings into unique slowness logs. Field processing products are basic and advanced processing products, such as the anisotropy analysis can be requested at a later stage.

- **Spectral Gamma Ray** (SGR, from the HNGS – Hostile Natural Gamma Ray Sonde). In addition to the total gamma ray, the HNGS measures the energy spectrum of the formation gamma rays. As the three main radioactive elements (potassium, thorium and uranium) are characterised by a different gamma energy, the tool can quantify those elements' content. Those concentrations can be used to quantify potassium-, uranium- or thorium-rich minerals (e.g. different clay minerals, potassic feldspars, organic matter, phosphates). The HSGR log is the sum of potassium, thorium and uranium gamma ray contributions to the total spectral gamma ray. Note that the total gamma ray from the GR and SGR tools are not necessarily quantitatively equivalent because these tools use different detectors, technologies, tool housing and calibrations. The HCGR log is the result of the HSGR log without the uranium contribution. The shading from HCGR to HSGR in log plots helps identify zones that may contain uranium-bearing organic matter and phosphates.

- **Spontaneous Potential** (SP). The SP log is a continuous measurement of the electric potential difference between an electrode in the SP tool and a surface electrode. Adjacent to shales, SP readings usually define a straight line known as the shale baseline. Next to permeable formations, the curve departs from the shale baseline; in thick permeable beds, these excursions reach a constant departure from the shale baseline, defining the "sand line". The deflection may be either to the left (negative) or to the right (positive), depending on the relative salinities of the formation water and the mud filtrate. If the formation water salinity is greater than the mud filtrate salinity (the more common case), the deflection is to the left. The movement of ions, essential to develop an SP, is possible only in rocks with some permeability, a small fraction of a millidarcy is sufficient. There is no direct relationship between the magnitude of the SP deflection and the formation's permeability or porosity.

- **Temperature** (TMP). The temperature log is acquired with the EMS tool that includes a temperature sensor. It is a measurement of the temperature in the borehole environment; thus, it is largely influenced by the temperature of mud. Since the temperature is affected by material outside the casing, a temperature log is sensitive to not only the borehole but also the formation and the casing – formation annulus. Mud temperature is generally less than that of fluids in the formation, but the temperature of the static mud is assumed to converge to the formation temperature after an infinite time. In practice, temperature logs are acquired several times after the last mud circulation, and the formation temperature is modelled based on the observed trend of temperature vs. time at each depth. On one hand, the temperature log is interpreted by looking for larger scale anomalies, or departures, from a reference gradient. This can give indications for permeable zones with fluid flow or for flow barriers hindering cross formational flow. On the other hand, localised smaller scale anomalies may correspond to the entry of borehole mud in the formation or fluid flow from the formation to the borehole. The temperature log should be interpreted together with structural geology, hydrogeology, and the other logs (e.g. images, resistivity logs).

3.2 Log data quality

3.2.1 Quality control procedures

Quality control (QC) of log data is important to guarantee their accuracy, repeatability, traceability, relevance, completeness, sufficiency, interpretability, clarity and accessibility. The generic QC procedures that were followed for each log dataset are presented as follows:

1. Digital data in .dlis format are loaded into a petrophysics software (Paradigm – Geolog) and checked for completeness (Are principal log channels, parameters and constants given?) and accessibility (Do the data load correctly when imported? Is the depth sampling rate steady and valid?).
2. Sufficient data: Do the first and last readings correspond to the interval of logs laid-out in the work programme?
3. Depth match is checked versus reference run. First run in hole is by convention, the reference for subsequent runs. GR log of the EDTC tool is always used for depth correlation because it has an excellent vertical resolution and sufficient character. Schlumberger depth matches data in the field but sometimes additional depth matching is required during QC. Such depth shifts are recorded in App. A6 – Table of depth shifts.
4. Are the calipers well calibrated? This is checked by comparing caliper measurements against the nominal inner diameter of the casing.
5. Borehole shape is checked: Are there washouts? Is the borehole on gauge? Undergauge? Ovalised? Are there breakouts? When the borehole shape is not gauge, the log quality can be degraded.
6. Does the cable tension show any overpulls or stick and pull events? These events can cause a locally discontinuous depth log measurement and alter the tool positioning which impacts log quality.
7. Graphic files (log plots) are checked for completeness, consistency and accuracy. In particular, the following sections of the graphic files are checked:
   - 7.1 Header: e.g. logging date, run number, mud parameters
   - 7.2 Borehole sketch and size / casing record: hole bit sizes and depths, casing sizes, weight and depth
   - 7.3 Borehole fluids: accuracy of mud physical parameters
   - 7.4 Remarks and equipment summary: serial numbers of equipment, completeness and accuracy of remarks
   - 7.5 Depth control parameters: right depth control policy and log of reference
   - 7.6 Summary of run passes: top and bottom of pass, automatic bulk shift applied
   - 7.7 Log (content and display): mnemonics, description, unit, scale, colour and label of logs; display of logs, log quality control (LQC) or data copy indicator curves provided (if applicable)

7.8 Parameters are checked including channel processing and tool control: corrections or offsets applied to measurements, modes of acquisition etc.

7.9 Calibration reports are checked for completeness and tolerances

8. Data repeatability for main vs. repeat passes (or downlog pass if applicable) is checked for a selection of important logs.
9. Were required, environmental corrections applied with the correct parameter values (e.g. mud salinity, mud weight, drill bit size, tool standoff, pressure / temperature).
10. Were processing parameters correctly applied (e.g. ECS minerals model options, MSIP time windows, APS lithology conversions)?
11. Data consistency is checked, including a comparison with logs from other runs via log plot and crossplots and the description of the cuttings for lithology. Are logs representative of expected lithologies and do they respond consistently?
12. Are orientation, accelerometer and magnetometer data accurate? This is essential for all data-sets that need to be oriented (e.g. borehole imagery [FMI/UBI], dipole sonic).
13. Mud resistivity and borehole temperature are checked for repeatability and checked against collected mud samples and thermometers in the logging head.
14. Quality of automatic picking on processing products (if applicable), e.g. compressional and shear wave slowness on semblance projections for sonic logs.

3.2.2 Bad-hole flags

To complete the data QC process, bad-hole flags were created to highlight zones where the log quality was degraded by 'bad-hole' conditions and should be viewed with caution. The methodology is presented in Tab. 3-1 and explained in detail in Appendix A.7 – Bad-hole flags.

Bad hole is a common issue with logging. It means that the borehole conditions are inadequate for obtaining optimum quality petrophysical logs that truly represent the formation that is being logged. The tools that either measure petrophysical properties in a space volume or must be in continuous contact with the borehole wall during logging (eccentred tools) are the most affected by bad hole. Washouts and rugose hole are the most common features that degrade the quality of the logs resulting for example in the underestimation of density and overestimation of sonic slowness.

Tab. 3-4: Bad-hole flag methodology

Bad-hole logic	**Logs used**	**Cutoff/method**
Overgauge flag	Caliper	Borehole diameter is greater than 115% of nominal drill bit size
Rugosity flag	Density correction (HDRA), acquired with TLD	The density correction log is calculated from the difference between the short- and long-spaced density measurements, an indicator of borehole rugosity and density quality. Density is not reliable when HDRA > 0.025 g/cm^3
Neutron standoff	Neutron standoff (STOF), acquired with APS	Neutron tool should be flushed with borehole wall or should have pre-determined physical standoff. If unintentional standoff, STOF > 0.35", bad hole is flagged
Density-neutron flag	Density (RHOZ) and neutron (APLC)	Systematic identification of outliers in density-neutron crossplot and comparison with analogue data from adjacent boreholes (e.g. Benken)

3.3 Composite log generation

The objective of the composite log dataset is to provide a traceable quality-controlled, edited, corrected and merged dataset for all petrophysical logging data recorded across the entire length of the borehole. Petrophysical tools acquire many logs that are not directly related to petrophysical properties but are needed to control that the tool sensors worked well (e.g. mechanical or electronics status of the sensors). In addition, some logs are acquired several times in a section (e.g. GR, Temperature). GPCI selects a collection of the most relevant logs for formation evaluation, correlation and calibration with core or seismic data. Some 65 representative logs are thus extracted for each borehole section. These logs are:

1. quality controlled (procedures in Section 3.2.1)
2. edited e.g. to keep data points that are true responses of the borehole and formation environment
3. further corrected for the borehole environment or artefacts
4. merged into composite logs that cover the entire or most of the borehole
5. The generated composite log dataset is generated and delivered in standard digital (LAS – Log ASCII Standard) and graphic (PDF log plot) format.

A more detailed procedure for the generation of the composite log is detailed in the next subchapter. In addition, a complete report in Excel format is provided (see Appendix A) which details all relevant information about the logs and the acquisition runs. Appendix A.5 – Composite log generation worksheet specifically details how the composite log dataset was generated through merging techniques.

3.3.1 Generic process

The following steps were conducted to generate composite log dataset:

1. A bit size log was generated according to the borehole design at the time of logging (see Appendix A.1 – Borehole design).
2. Logs were depth-shifted as required (see Appendix A.8 – Post-acquisition depth shifts).
3. First and last readings were edited to remove values acquired before the tool sensors started reading the borehole (e.g. constant values just before/after the sensor is switched off/on) and/or before the tools started to move upward (e.g. stationary measurements close to total depth). Log readings were further edited if they did not read the borehole formation environment, e.g. logs can be impacted by the nearby casing shoe and cement, become decentralised when there are changes in the borehole diameter, or sediment infills at bottom of the borehole.
4. All logs that were not valid in cased hole were discarded. For the TRU1-1 composite log dataset, this included all logs except for the total gamma ray log (ECGR_EDTC) from the EDTC and borehole temperature (TMP) from the EMS.
5. Bad-hole flags were created based on advanced log analysis to highlight zones where the log quality was affected by bad-hole conditions.
6. Total gamma ray log (ECGR_EDTC) was corrected for the radioactive potassium silicate in the drilling mud using the borehole potassium corrected total spectral gamma ray log (HSGR) for calibration. It was further normalised to account for attenuated readings in cased hole intervals according to standard practice. The corrected gamma ray log was then renamed GR_KCOR.
7. Poor quality sonic slowness data (DTCO, DTSM) caused by imprecise automatic picking were removed and interpolated where applicable.
8. The edited and corrected logs from each section were merged. Merging points were chosen carefully to optimise log coverage and composite log consistency. See Appendix A.5 – Composite log generation.
9. Standardised log names, units and descriptions were used.
10. Logs acquired at higher resolution (e.g. RHO8, PEF8 have sample rates 0.0508 m – ⅙ ft) were resampled to the standard rate of 0.1524 m (½ ft), because the digital LAS format cannot support mixed sample rates.
11. Final log plots at a scale of 1:200 m MD and 1:1'000 m MD were produced in PDF graphic file format along with digital data in LAS format.

Tab. 3-2 lists and describes all the log curves / channels that are provided in the composite log set.

Tab. 3-5: Composite log LAS channel listing

Curve / channel	**Units**	**Description**
DEPTH	M	
APLC	V/V	Near/array Corrected Limestone Porosity (Epithermal HI)
BS	IN	Bit Size
DEVI	DEG	Borehole deviation
DTCO	US/F	Delta-T Compressional
DTSM	US/F	Delta-T Shear
DTST	US/F	Delta-T Stoneley
DWAL_WALK2	W/W	Dry Weight Fraction Pseudo Aluminium (SpectroLith WALK2 Model)
DWCA_WALK2	W/W	Dry Weight Fraction Calcium (SpectroLith WALK2 Model)
DWCL_WALK2	KGF/KGF	Dry Weight Fraction Chlorine Associated with Salt (SpectroLith WALK2 Model)
DWFE_WALK2	W/W	Dry Weight Fraction Iron + 0.14 Aluminium (SpectroLith WALK2 Model)
DWGD_WALK2	PPM	Dry Weight Fraction Gadolinium (SpectroLith WALK2 Model)
DWHY_WALK2	KGF/KGF	Dry Weight Fraction Hydrogen Associated with Coal (SpectroLith WALK2 Model)
DWSI_WALK2	W/W	Dry Weight Fraction Silicon (SpectroLith WALK2 Model)
DWSU_WALK2	W/W	Dry Weight Fraction Sulphur (SpectroLith WALK2 Model)
DWTI_WALK2	W/W	Dry Weight Fraction Titanium (SpectroLith WALK2 Model)
FLAG_BADHOLE_OVERGAUGE		Overgauge Borehole Bad-Hole Flag
FLAG_BADHOLE_RUGO		Rugose Borehole Bad-Hole Flag
FLAG_BADHOLE_STOF		Neutron Porosity Standoff Bad-Hole Flag
FLAG_UNFIT_ND		Flag that indicates unfit neutron-density data for deterministic log evaluation
FPLC	V/V	Near/Far Corrected Limestone Porosity (Thermal HI)
GR_KCOR	GAPI	Total natural radioactivity corrected for the borehole potassium (EDTC)
HAZI	DEG	Borehole azimuth
HCGR	GAPI	HNGS Computed Gamma Ray
HDAR	IN	Hole Diameter from Area
HDRA	G/C3	Density Standoff Correction
HFK	%	HNGS Formation Potassium Concentration
HSGR	GAPI	HNGS Standard Gamma-Ray
HTHO	PPM	HNGS Formation Thorium Concentration
HURA	PPM	HNGS Formation Uranium Concentration
PEF8	B/E	High Resolution Formation Photoelectric Factor
PEFZ	B/E	Standard Resolution Formation Photoelectric Factor
RD1	IN	Radius 1

Tab. 3-2: continued

Curve / channel	**Units**	**Description**
RD2	IN	Radius 2
RD3	IN	Radius 3
RD4	IN	Radius 4
RD5	IN	Radius 5
RD6	IN	Radius 6
RHGE_WALK2	G/CC	Matrix Density from Elemental Concentrations (SpectroLith WALK2 Model)
RHO8	G/C3	High Resolution Formation Density
RHOZ	G/C3	Standard Resolution Formation Density
RLA0	OHMM	Apparent Resistivity from Computed Focusing Mode 0
RLA1	OHMM	Apparent Resistivity from Computed Focusing Mode 1
RLA2	OHMM	Apparent Resistivity from Computed Focusing Mode 2
RLA3	OHMM	Apparent Resistivity from Computed Focusing Mode 3
RLA4	OHMM	Apparent Resistivity from Computed Focusing Mode 4
RLA5	OHMM	Apparent Resistivity from Computed Focusing Mode 5
RT_HRLT	OHMM	HRLT True Formation Resistivity
RXO8	OHMM	Invaded Formation Resistivity filtered at 8 inches
RXOZ	OHMM	Invaded Formation Resistivity filtered at 18 inches
RXO_HRLT	OHMM	HRLT Invaded Zone Resistivity
SIGF	CU	Formation Capture Cross-Section
SP	MV	Spontaneous Potential
STOF	IN	Effective Standoff in Limestone
SV	MPa	Overburden vertical stress (Sv)
TMP	DEGC	Mud Temperature
U8	B/C3	High Resolution Volumetric Photoelectric Factor
UZ	B/C3	Volumetric Photoelectric Factor
WANH_WALK2 *	W/W	Dry Weight Fraction Anhydrite / Gypsum (SpectroLith WALK2 Model)
WCAR_WALK2 *	W/W	Dry Weight Fraction Carbonate (SpectroLith WALK2 Model)
WCLA_WALK2 *	W/W	Dry Weight Fraction Clay (SpectroLith WALK2 Model)
WCOA_WALK2 *	W/W	Dry Weight Fraction Coal (SpectroLith WALK2 Model)
WEVA_WALK2 *	W/W	Dry Weight Fraction Salt (SpectroLith WALK2 Model)
WPYR_WALK2 *	W/W	Dry Weight Fraction Pyrite (SpectroLith WALK2 Model)
WQFM_WALK2 *	KGF/KGF	Dry Weight Fraction Quartz+Feldspar+Mica (QFM) (SpectroLith WALK2 Model)
WSID_WALK2 *	W/W	Dry Weight Fraction Siderite (SpectroLith WALK2 Model)

* Qualitative data should only be used as a lithology indicator.

3.3.2 Gaps in log coverage

Optimising the petrophysical log and MHF testing coverage was an objective of the logging and testing campaigns, in particular for the potential Opalinus Clay rock host. Despite best efforts, gaps in log coverage are an inherent limitation in wireline logging operations.

Complete log coverage at changes in drilling section is possible if the acquisition of the lowermost part of the drilling section is repeated later with the acquisition of the uppermost part of the drilling section below. Logs acquired with the same sensor, which overlap over two sections can then be merged providing complete coverage. This is not always possible due to limitations related to tool string geometry, borehole conditions and borehole design. Examples include:

- Cuttings infill the bottom of the hole preventing the tool string from reaching total depth.
- The tool string should not tag the bottom hole with certain fragile tools (e.g. UBI).
- The offset of the sensors relative to the bottom of the tool string
- The rathole clearance (space between casing shoe and the bottom of the drilled hole) available for logging in the section below is too short. If the casing shoe is too close to the bottom of the section and the lowermost part of the open hole was not logged before casing installation, some log coverage will be lost.
- The rathole available for logging in the section below is first enlarged, and its diameter is different (e.g. 17½") from that of the cored section below (6⅜"). Abrupt changes in borehole size are not favorable for logging because they are often associated with bad hole and eccentred tools in contact with the borehole wall acquire logs of degraded quality, causing gaps in log coverage.

The above factors were taken into consideration in the design of work programs. For each logging campaign, project guidelines defined the balance between the optimisation of log coverage (short tool strings, more runs, longer campaign) and saving rig time and associated costs (slightly longer tool strings, less runs, shorter campaign).

For the main drilling sections where petrophysical logs were acquired, a summary of the meterage of logged data and the percentage of total depth this data represents, is summarised in Tab. 3-3. The Opalinus Clay and bounding formations (Dogger – Lias) were examined in greater detail. Almost complete log coverage was acquired, with only relatively small gaps (most less than 5 m) in log coverage between borehole sections. Spectral GR logs (HNGS tool) have only 93.2% coverage, because the formation at the bottom of the borehole often became activated by the radioactive source of the ECS tool.

Tab. 3-6: Summary of Petrophysical Log Coverage from Drilling Section II to TD

Measurement	**Section II to TD** (498 m – 1'310 m MD)		**Opalinus Clay and Bounding Formations (Dogger – Lias)** (725.03 m – 971.55 m MD)	
	Meterage	**Coverage**	**Meterage**	**Coverage**
Caliper	788.54	97.1%	246.52	100.0%
Borehole orientation	782.57	96.4%	245.52	99.6%
Total Gamma Ray	803.50	99.0%	240.81	97.7%
Spontaneous Potential	784.26	96.6%	246.52	100.0%
Spectral Gamma Ray	731.38	90.1%	229.76	93.2%
Density	764.64	94.2%	245.86	99.7%
Photoelectric Factor	765.66	94.3%	245.71	99.7%
Microresistivity	759.17	93.5%	245.81	99.7%
Neutron (NHI)	759.26	93.5%	245	99.4%
Sigma Formation Capture Cross-Section	764.59	94.2%	245	99.4%
Resistivity	755.95	93.1%	238.24	96.6%
Sonic	758.57	93.4%	238.44	96.7%
Element Spectroscopy	789.14	97.2%	246.52	100.0%
Ultrasonic Borehole Imagery	755.30	93.0%	245.5	99.6%
Microresistivity Borehole Imagery	775.00	95.4%	246.52	100.0%

The depths at which there were gaps in log coverage in the final composite dataset are detailed in Appendix A.5 – Composite log generation.

3.4 Petrophysical logging results and description

The main features of the petrophysical logs of the composite dataset are described below by litho-stratigraphic units.

3.4.1 Cenozoic: Quaternary, OMM, USM, and Siderolithikum (0 to 474 m MD)

The Molasse, Siderolithic and transition to Malm units in open hole Section I of the borehole were logged with a limited suite of logging tools: total GR, density, compressional sonic and inclinometer.

The large diameter hole (23") was at the mechanical specification limits for the open hole logging tools (TLD: 22"; MSIP: 22"). In addition, the borehole wall was rugose and the hole size was slightly in overgauge. Thus, log quality was generally poor and only the total GR (GR_KCOR) provided semi-quantitative log response (Fig. 3-1). The quality of the density log was insufficient for petrophysical analysis and was thus disregarded. Sonic (DTCO) should be used with care, e.g. as a stratigraphic marker for correlation.

GR_KCOR typically ranged from 47 to 94 GAPI, which indicates moderate but variable clay contents. A few radioactive streaks up to 194 GAPI were observed e.g. at 189 and 306.8 m MD. They suggest the presence of organic matter.

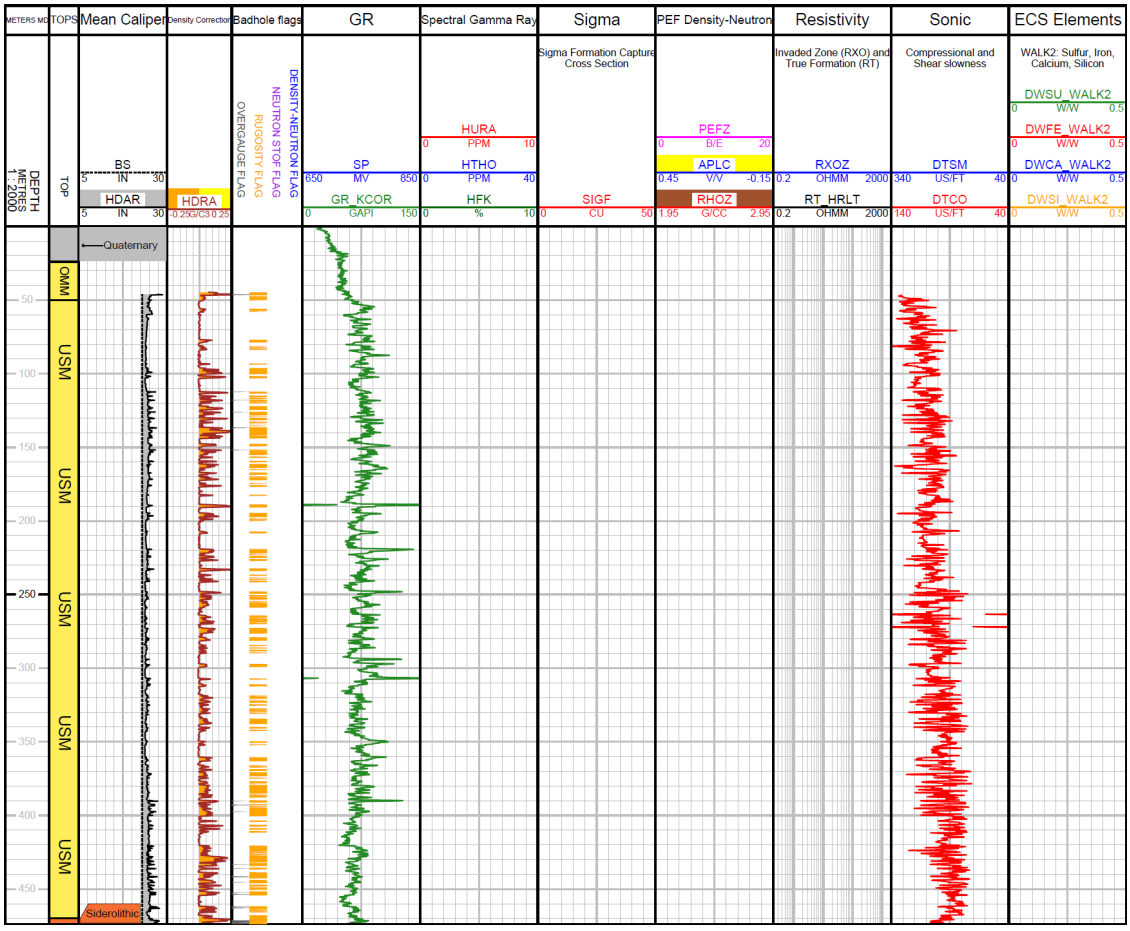

Fig. 3-2: Main logs of the composite dataset in the Cenozoic units

3.4.2 Malm: «Felsenkalke» + «Massenkalk» to Wildegg Formation (474 to 725.03 m MD)

GR and sonic were the only valid wireline logs that were acquired in the top of the Malm during Section I wireline logging (inclinometer data are not discussed). Both logs show sharp changes in their values at the Tertiary / Malm transition, shifting towards lower GR and sonic slowness values (Fig. 3-2), implying low clay content and fast acoustic wave propagation indicative of limestone.

Log responses reflect the borehole lithology well, except for some bad-hole zones in the «Felsenkalke» + «Massenkalk», where the borehole wall rugosity deteriorated the response of the TLD tool logs (density and microresistivity).

Logs in the Malm units have an overall similar log signature characterised by:

- Generally low clay content except in the Schwarzbach and Wildegg Formations: low total GR (GR_KCOR: 0 to 35 GAPI), spectral GR (e.g. thorium HTHO: < 3 ppm) and sigma (SIGF: 7.2 to 17 CU). Clay content increases in the Schwarzbach Formation (GR_KCOR: 17 to 63 GAPI) and the Wildegg Formation below 719 m MD.
- Calcite is the dominant mineral: an almost perfect overlap in the neutron-density limestone-compatible scale (density [RHOZ] and neutron [APLC] readings in pure limestone are 2.71 g/cm^3 and 0.0 v/v, respectively), the calcium dry weight fraction (DWCA) is close to that of pure calcite (0.394 W/W), as is the photoelectric factor (PEFZ) – pure calcite value of 5.1 B/E.
- In the low clay units, porosity is low, density is high (never lower than 2.51 g/cm^3; mean: 2.66 g/cm^3) and sonic (DTCO) rarely exceeds 64 µs/ft.

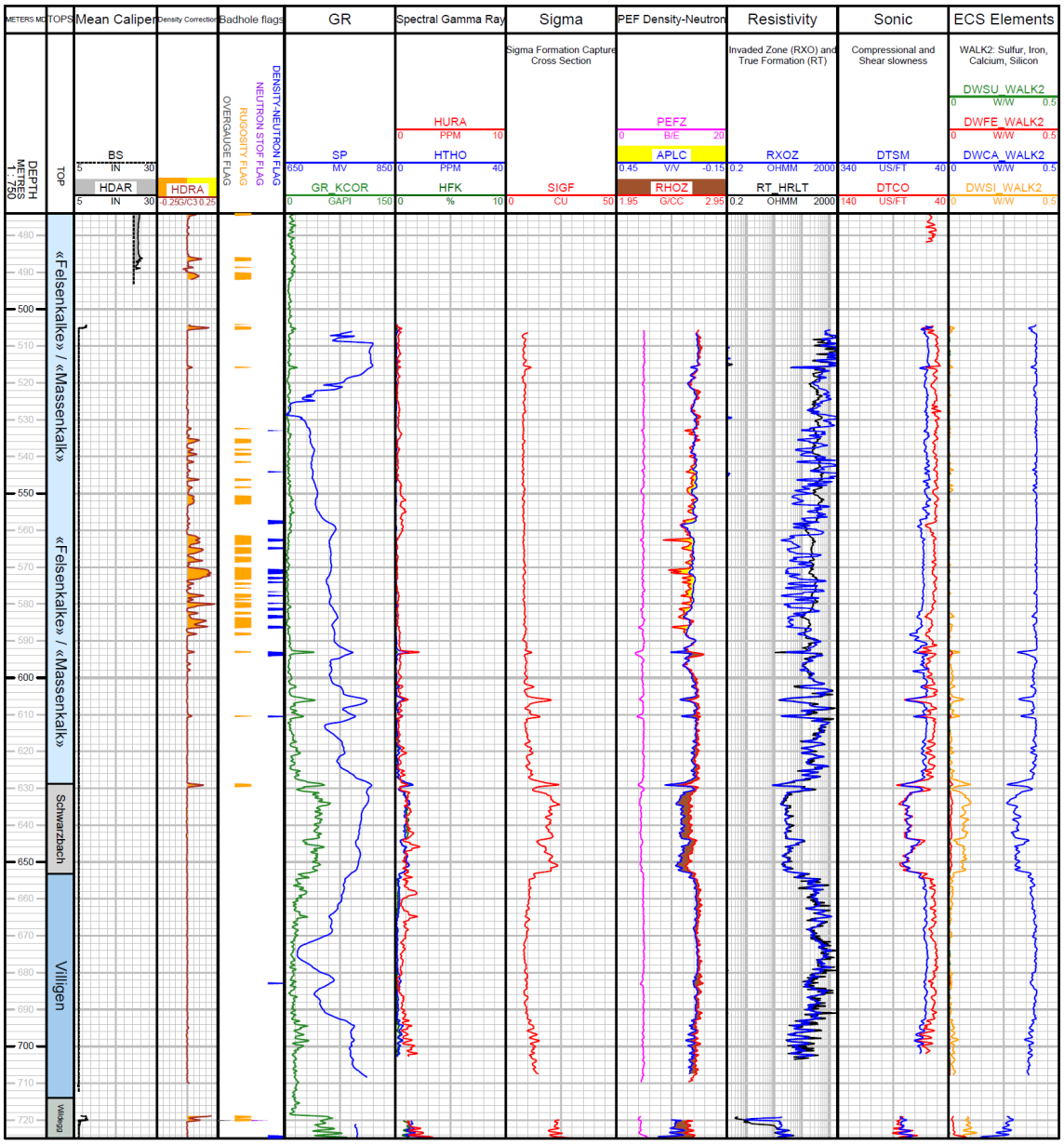

Fig. 3-3: Main logs of the composite dataset in the «Felsenkalke» + «Massenkalk» to Wildegg Formation

3.4.3 Wutach Formation to «Murchisonae-Oolith Formation» (725.03 to 816.43 m MD)

The top of the Dogger (Wutach Formation) can be identified by an increase in total GR, a wide separation in the neutron-density logs in a limestone-compatible scale and increase in iron concentration (DWFE), all indicative of siderite, iron oxide or hydroxide bearing rocks (Fig. 3-3).

Due to good-hole conditions, log responses reflect the borehole lithology well from the Wutach Formation to the «Murchisonae-Oolith Formation». Logs have the following attributes:

- Highly variable clay content that is moderate to low in parts of the Wedelsandstein Formation and high in the «Parkinsoni-Württembergica-Schichten» («Park.-W.-Sch») unit. Excluding the zones that contain siderite, iron oxides or hydroxides (DWFE < 0.05 W/W), the total GR ranges from 26 to 106 GAPI, SIGF from 12.9 to 37.3 CU and HTHO from 2.9 and 15 ppm. The «Humphriesioolith Formation» and Wedelsandstein Formation contain less clay than the «Park.-W.-Sch» unit above.

- The occurrence of siderite, iron oxide or hydroxide is typical in these formations. In the Wutach Formation, parts of the lower «Park.-W.-Sch» unit and the «Humphriesioolith Formation»: a wide separation in the neutron-density, high total and spectral GR (especially thorium HTHO up to 23 ppm and uranium HURA up to 4.2 ppm), high iron concentration (DWFE: above 0.05 W/W) and high photoelectric factor (PEFZ: above 4.5 B/E).

- The matrix mineralogy is dominated by calcite: in the lowest clay zones the PEFZ is in the range of 2.8 to 5.4 B/E, while calcium is relatively high (DWCA: up to 0.24 W/W; 0.394 W/W in pure calcite), which is typical of marls. In the Wedelsandstein Formation, the separation between neutron-density is quasi absent, an indication of pure limestone if calcite was the only matrix mineral, however, the clay content is moderate to low. This indicates a siliciclastic component in the matrix mineralogy, that is consistent with the rather high silicon concentration (DWSI: up to 0.31 W/W; 0.467 W/W in pure quartz).

- The spectral GR potassium (HFK) and thorium (HTHO) log signatures in the clay-rich units suggest that non-potassic smectite (e.g. montmorillonite) is the dominant clay type.

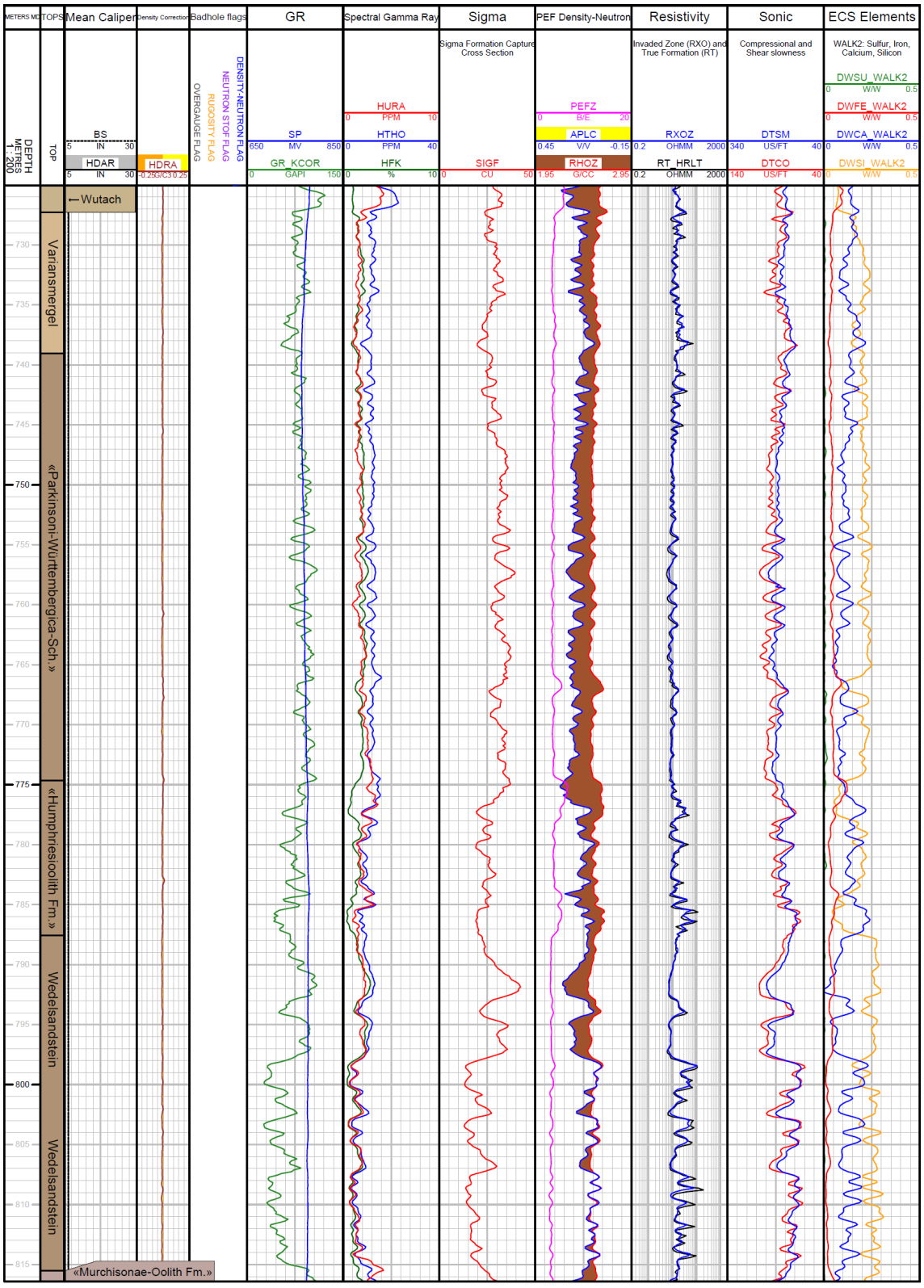

Fig. 3-4: Main logs of the composite dataset in the Wutach Formation to «Murchisonae-Oolith» unit

3.4.4 Opalinus Clay (816.43 to 927.87 m MD)

The top Opalinus Clay is characterised by an increase in clay content, as observed by the decrease in resistivity (e.g. RT_HRLT), a wider neutron-density separation in a limestone-compatible scale and significant decrease in calcium concentration (DWCA).

Log responses reflect the borehole lithology well because hole conditions were excellent for wireline logging. In the Opalinus Clay, logs have the following attributes (Fig. 3-4):

- Consistently moderate to high clay content: the total GR (GR_KCOR) ranges from 65 to 117 GAPI; sigma (SIGF) correlates very well (positively) to GR_KCOR, ranging from 26.8 to 44.1 CU; the compressional wave slowness DTCO was high (slow formation) and generally above 91 µs/ft; the density-neutron separation is typical of lithologies with high clay content.
- Several carbonate streaks can be observed at 825.1, 832.9, 844.7 and 859.9 m MD characterised by: an increase in density and decrease in neutron with values approaching those of pure calcite (RHOZ: 2.71 g/cm^3; APLC: 0.0 v/v); an increase in calcium (DWCA up to 0.14 W/W); an increase in resistivity logs (e.g. RT_HRLT).
- While the clay content is relatively homogeneous throughout, two distinct trends can be observed. In the upper part of the formation above 874 m MD, they remain rather constant except where carbonates streaks are observed. Below 874 m MD, the clay content gradually increases with depth as shown by the gradual widening of the density-neutron separation and increase in sigma. Carbonate streaks are absent or insignificant in the lower part of the formation.
- The spectral GR potassium (HFK) and thorium (HTHO) log signatures in the clay-rich units suggest that non-potassic smectite (e.g. montmorillonite) is the dominant clay type.
- Matrix mineralogy is complex. Both calcium (DWCA) and silicon (DWSI) concentrations are often higher than those in smectite clays (DWCA: 0.00 to 0.10 W/W; DWSI: 0.16 to 0.28 W/W; excluding the carbonate streaks), which suggests siliciclastic and carbonate components in the matrix.

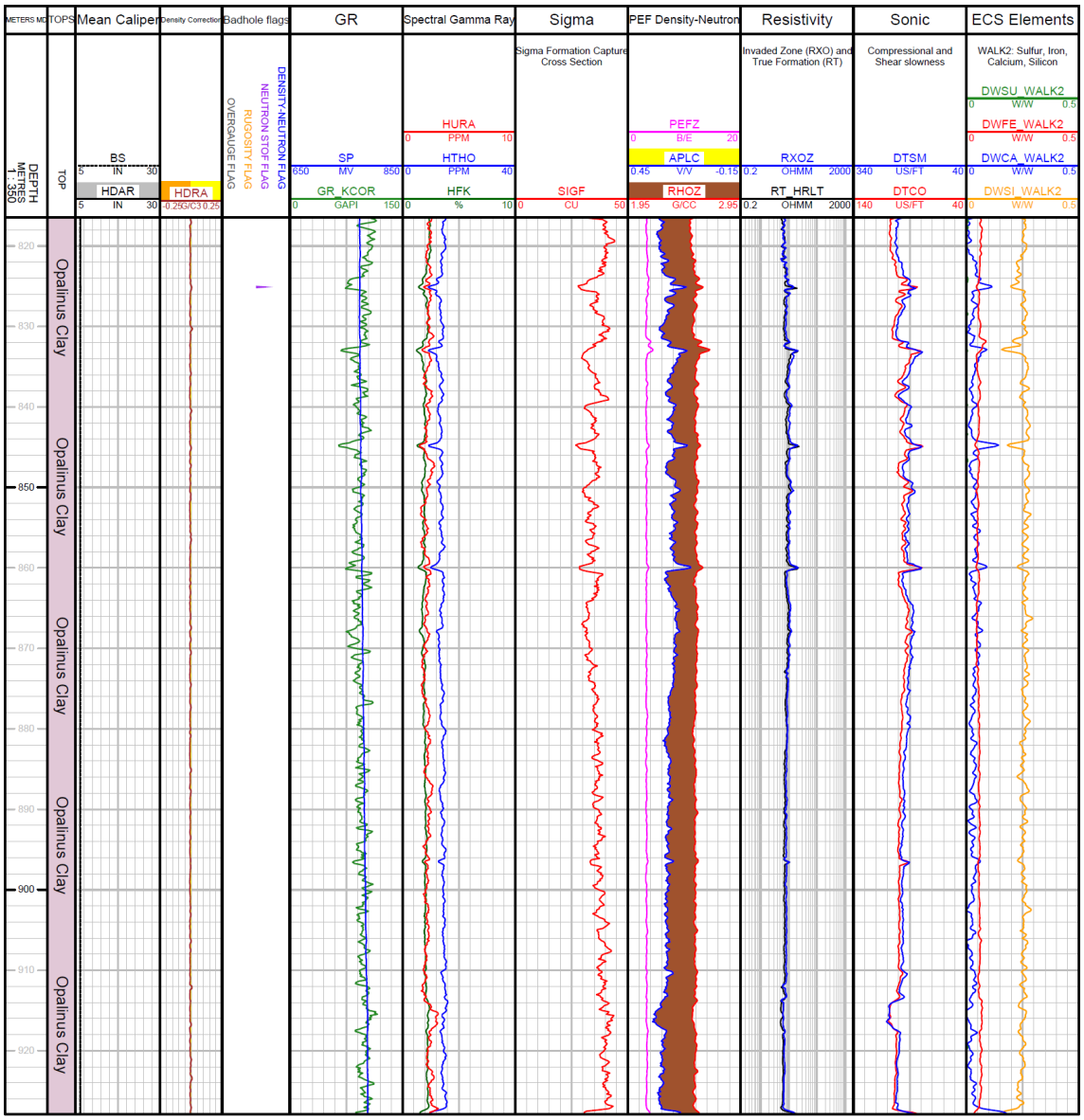

Fig. 3-5: Main logs of the composite dataset in the Opalinus Clay

3.4.5 Staffelegg Formation (927.87 to 971.55 m MD)

The transition between the Dogger and the Lias (Staffelegg Formation) is gradual from 927.2 to 928.2 m MD. The top of the Staffelegg Formation can be identified by the decrease in clay content as shown by the total GR (GR_KCOR), thorium (HTHO), sigma (SIGF) and the density-neutron separation (Fig. 3-5).

Hole conditions were good in the Staffelegg Formation. Logs respond well to the borehole lithology having the following attributes:

- Highly variable clay content: total GR (50 to 166 GAPI), sigma (16.7 to 41.7 CU) and thorium (5.1 to 15.6 ppm), e.g. low clay content in the Beggingen Member (961.94 to 965.66 m MD) but intermediate to high clay content in the Frick Member (949.76 to 961.94 m MD).
- Organic matter is likely present: the high total GR zones (GR_KCOR > 105 GAPI) correspond with the uranium peaks (HURA: up to 10.4 ppm).
- Pyrite is an important accessory mineral in several members of the Staffelegg Formation (Gross Wolf, Rietheim and Grünschholz Members): Sulphur concentration (DWSU) ranges from 0 to 0.03 W/W; the photoelectric factor (PEFZ), a reactive marker of pyrite, reaches high values of 5.7 B/E.
- Matrix mineralogy is dominated by carbonate: calcium (DWCA) varies between 0 and 0.30 W/W (pure calcite: 0.394 W/W); however, mineralogy remains complex, the multi-mineral interpretation detailed in Dossier X will help to better understand this complex mineralogy.

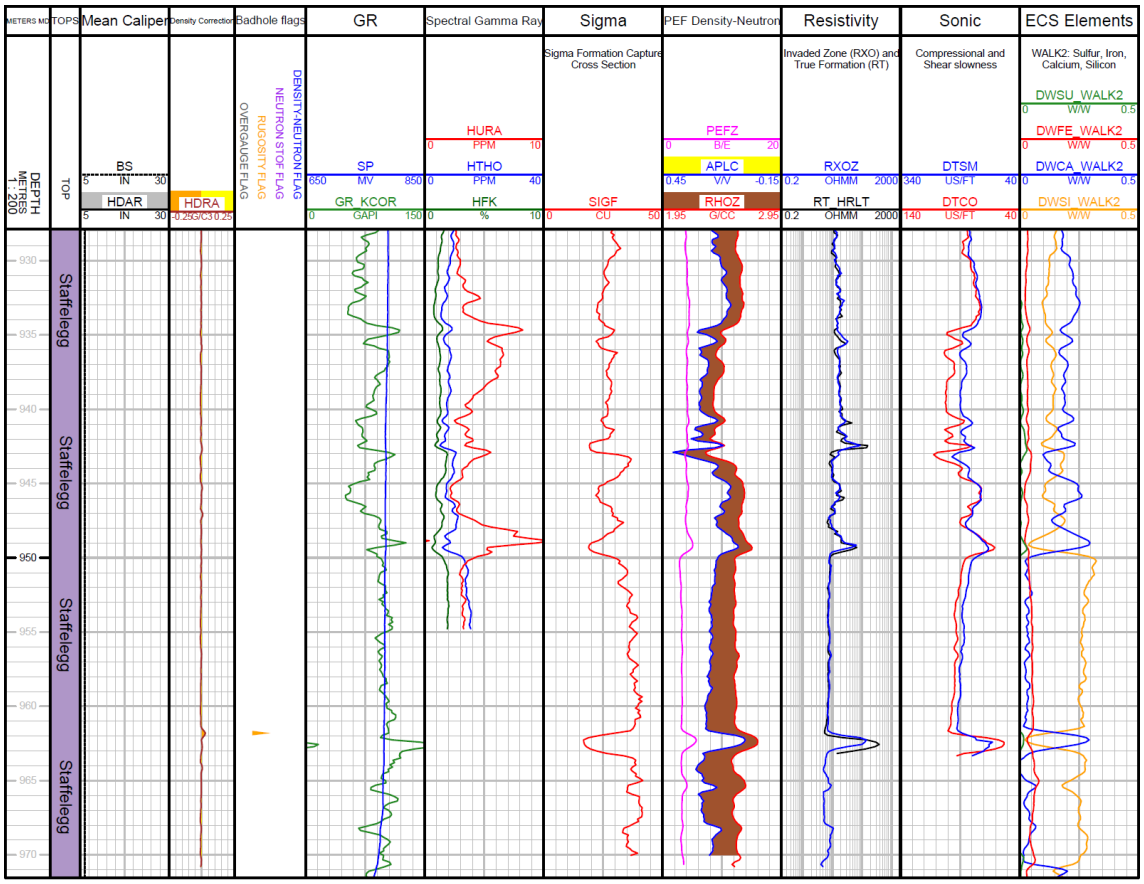

Fig. 3-6: Main logs of the composite dataset in the Staffelegg Formation

3.4.6 Klettgau Formation (971.55 to 1'027.44 m MD)

The top of the Triassic (Klettgau Formation) could not be logged in open hole because the rathole clearance below Section III was insufficient. Thus, only the total GR (GR_KCOR) was acquired (through the casing) in the Belchen Member (971.55 to 972.94 m MD) and the upper part of the underlying Gruhalde Member.

Hole conditions were degraded in most of the formation as indicated by the bad-hole flags (Fig. 3-6). Bad-hole conditions affected log responses to lithology, particularly the density (RHOZ) and neutron (APLC) logs. Logs in the Klettgau Formation show the following attributes:

- Highly variable clay content: total GR ranges from 2 to 196 GAPI, sigma from 8.7 to 46 CU and thorium from 0.1 to 14.8 ppm; clay indicators have a bimodal distribution that reflect zones with low clay content (from 990.2 to 1'004.4 m MD: Seebi Member; 1'013.3 to 1'015.7 m MD: Gansingen Member), and zones with intermediate to high clay contents (971.55 to 990.2 m MD: Belchen and Gruhalde Members; 1'004.4 to 1'013.3 m MD: Gruhalde Member; 1'015.7 to 1'027.44 m MD: Ergolz Member).
- Carbonate is the main matrix mineral in the upper Klettgau Formation down to 999.4 m MD, indicated by the intermediate to high calcium concentration (DWCA: 0.10 to 0.39 W/W; pure calcite: 0.394 W/W). The carbonate has a dolomitic signature, as shown by the photoelectric factor (PEFZ) whose mean value (3.5 B/E) is close to that of pure dolomite (3.1 B/E).
- In the intervals 999.4 to 1'013.3 m MD and 1'015.7 to 1'027.44 m MD, the calcium concentration is low (mean DWCA: 0.05 W/W) and the silicon concentration increases up to 0.41 W/W, this is also true of the zones with low clay content. This suggests that the matrix mineralogy is dominated by siliciclastic minerals such as quartz. The density-neutron "cross-over" (density is to the left of neutron in the limestone-compatible scale: yellow shading), also supports the presence of quartz e.g. from 1'001.3 to 1'003.9 m MD.
- In between these two quartz intervals, high sulphur (DWSU: up to 0.23 W/W) and low iron (DWFE) concentrations are present in the Gansingen Member (from 1'013.3 to 1'015.7 m MD), which suggests a unit composed of anhydrite (pure anhydrite: 0.234 W/W sulphur).
- Organic matter is likely present: the high total GR zones (GR_KCOR > 145 GAPI) correspond with the uranium peaks (HURA: up to 8.1 ppm).

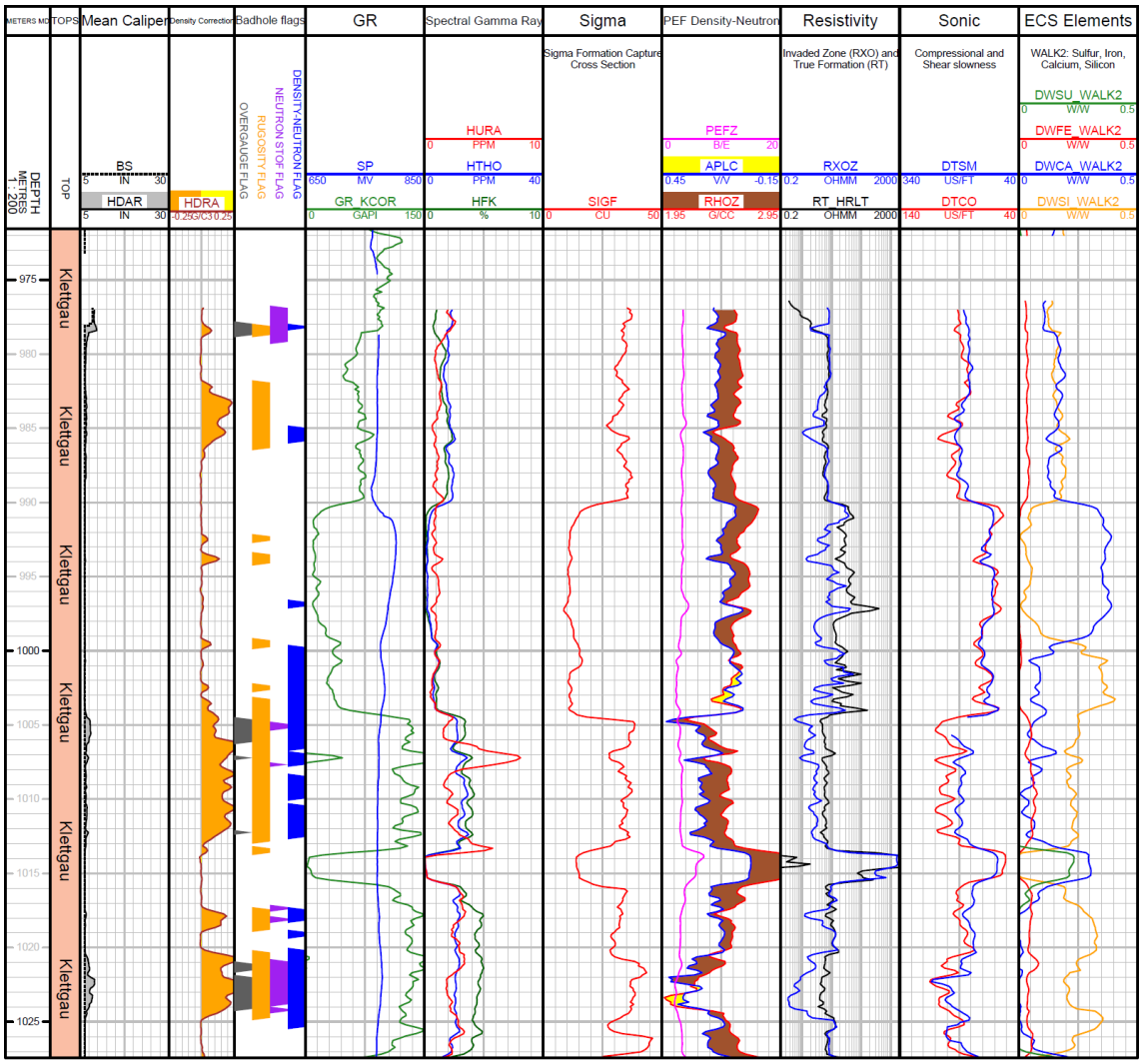

Fig. 3-7: Main logs of the composite dataset in the Klettgau Formation

3.4.7 Bänkerjoch Formation (1'027.44 to 1'084.22 m MD)

The top of the Bänkerjoch Formation is characterised by a shift to lower values of total GR (GR_KCOR), potassium (HFK) and sigma (SIGF). At the same time, sulphur (DWSU) and calcium (DWCA) concentrations increase. These log characteristics show the onset of the significant concentrations of anhydrite of this formation.

Hole conditions were mostly good in the Bänkerjoch Formation and logs responded well to borehole lithology. Logs show the following attributes (Fig. 3-7):

- Rapid variations in most logs at the metre scale or less, which suggests two main alternating lithologies. One having high sulphur (DWSU: up to 0.21 W/W) and calcium concentrations (DWCA: up to 0.34 W/W), high photoelectric factor (PEFZ: up to 5.2 B/E) and intermediate to low total GR which suggest predominantly anhydrite bearing beds. The alternate beds have higher clay contents as indicated by the lower sulphur and calcium concentrations, high silicon (DWSI: up to 0.26 W/W) and intermediate to high total GR.
- The density-neutron separation in the limestone compatible scale remains similar for both beds but logs shift from left to right for the clay and anhydrite dominant endmembers, respectively.
- Due to the limited vertical resolution of the logging tool, often higher than 10" (e.g. APS: 14"), the alternating lithologies are not necessarily correctly reflected in the logs. The logging tools average the physical and chemical properties over a fixed volume, which means that centimetre scale beds are represented as a mixture of anhydrite and clays for a given depth.

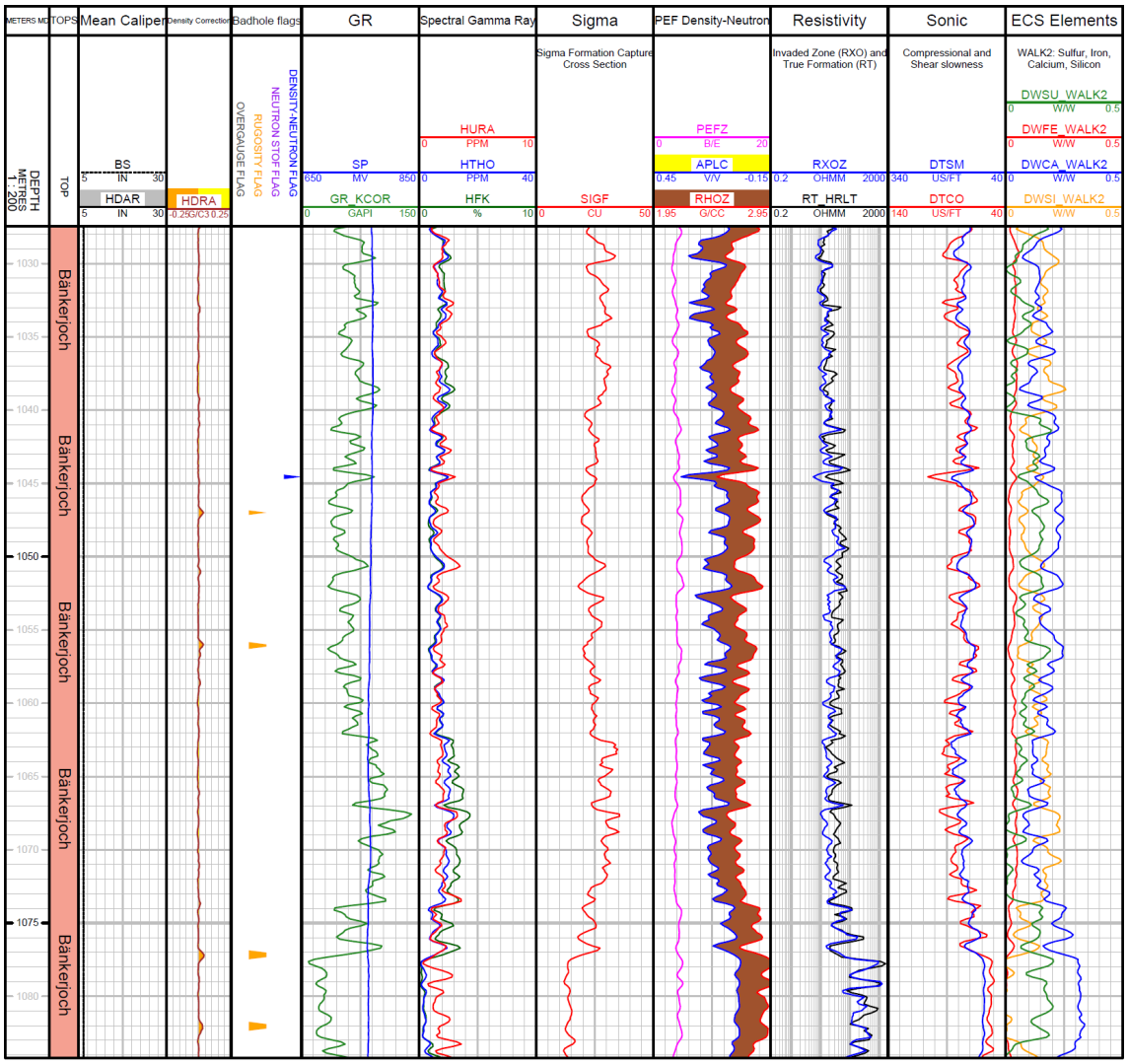

Fig. 3-8: Main logs of the composite dataset in the Bänkerjoch Formation

3.4.8 Schinznach Formation (1'084.22 to 1'154.43 m MD)

The top of the Schinznach Formation is identified by the disappearance of the sulphur content (DWSU) and a decrease in the photoelectric factor (PEFZ) below the lowest anhydrite bed of the Bänkerjoch Formation.

Due to the good-hole conditions, log responses reflect the borehole lithology well and are characterised by the following attributes (Fig. 3-8):

- Low to moderately low clay contents as shown by the total GR (GR_KCOR: 7 to 54 GAPI), sigma (SIGF: 7.0 and 12.2 CU) and thorium (HTHO: 0.4 to 4.1 ppm), except in the interval from 1'087.5 to 1'090.3 m MD and above 1'085.3 m MD where two clay-rich layers are present.
- Carbonate is the main matrix mineral as shown by the fast sonic (DTCO, DTSM), low silicon (DWSI) and high calcium concentrations (DWCA: up to 0.40 W/W; pure calcite is 0.394 W/W for comparison).
- From the top of the Schinznach Formation to 1'119 m MD, the carbonate has a dolomitic signature as shown by the photoelectric factor (PEFZ) whose mean value is the same as that of pure dolomite (3.1 B/E), whilst the density-neutron separation is positive and the clay content is low. The large separation between the shallow (RXOZ) and deep (RT_HRLT) resistivities indicate invasion of mud filtrate into the permeable formation.
- From 1'119 m MD to the bottom of the Schinznach Formation, the mean photoelectric value (4.5 B/E) is close to that of pure calcite (5.1 B/E) and the density-neutron separation is slightly positive or absent suggesting that the carbonates contain limestones and dolomitic limestones.

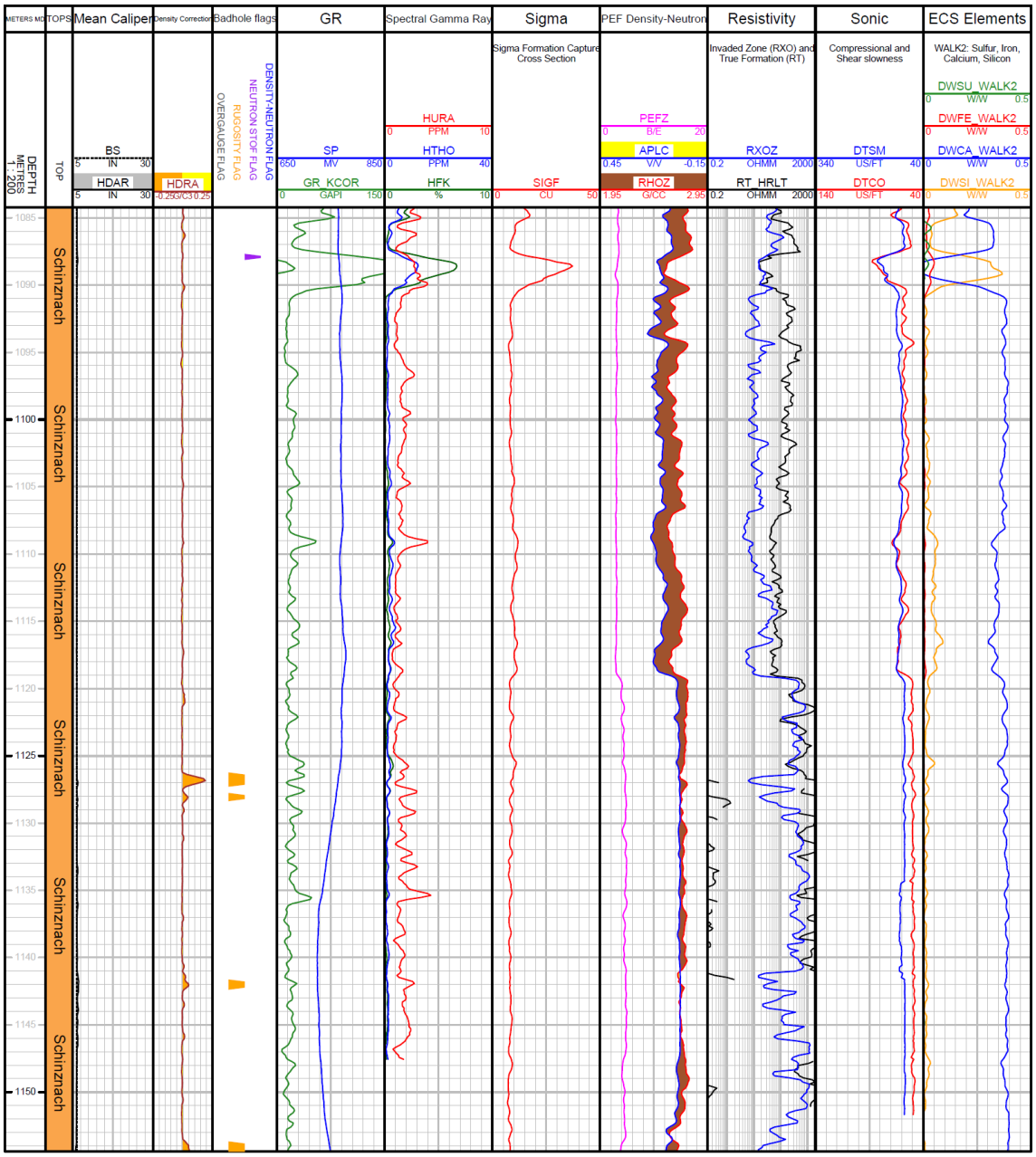

Fig. 3-9: Main logs of the composite dataset in the Schinznach Formation

3.4.9 Zeglingen Formation (1'154.43 to 1'204.5 m MD)

The top of the Zeglingen Formation corresponds to a decrease in calcium content (DWCA), an increase of silicon content (DWSI) and a reduction in the photoelectric factor (PEFZ).

Some logs have a gap in coverage between the lower Schinznach Formation and the upper Zeglingen Formation due to insufficient rathole clearance after Section IV drilling.

Hole conditions were good except in a short interval below the casing shoe (from 1'158.4 to 1'162.1 m MD), where there were washouts in the rathole. Outside the rathole, logs responded well to borehole lithology. The Zeglingen Formation was characterised by the following (Fig. 3-9):

- Low to moderate clay content: total GR (GR_KCOR: 5 to 113 GAPI), sigma (SIGF: 7.3 to 33.6 CU) and thorium (HTHO: 0.2 to 8.3 ppm).
- Density (RHOZ) is often greater than 2.9 g/cm^3 suggesting the presence of anhydrite. This is supported by the photoelectric factor (PEFZ) that is close to the value in pure anhydrite (5.05 B/E) and the significant sulphur content (DWSI: up to 0.24 W/W; value in anhydrite: 0.236 W/W).
- From the top of the Zeglingen Formation to 1'168.5 m MD, logs indicate less anhydrite, and dolomite is the main mineral component: the photoelectric factor values are close to that of pure dolomite (3.1 B/E) and calcium contents (DWCA) ranges from 0.18 to 0.39 W/W.

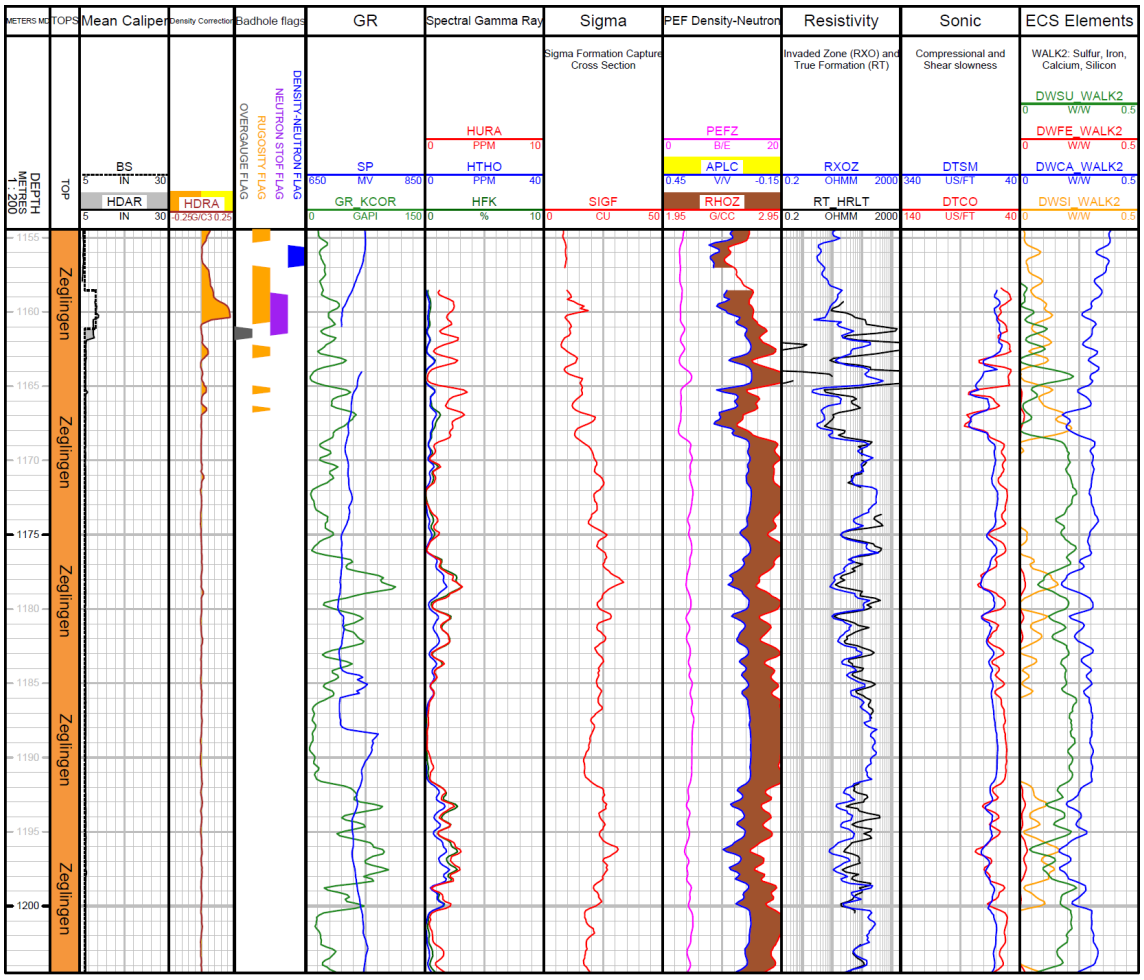

Fig. 3-10: Main logs of the composite dataset in the Zeglingen Formation

3.4.10 Kaiseraugst Formation (1'204.5 to 1'233.2 m MD)

The top of the Kaiseraugst Formation is difficult to identify because the wireline logs do not show any obvious markers. Nevertheless, a gradual increase is observed between 1'204 and 1'208 m MD as shown by the clay indicators (e.g. GR_KCOR).

Due to the good-hole conditions, log responses reflect the borehole lithology well (Fig. 3-10). Logs in the Kaiseraugst Formation have the following attributes:

- Intermediate to high clay content as shown by the total GR (GR_KCOR: 42 to 169 GAPI), sigma (SIGF: 19.1 to 38.9 CU) and thorium (HTHO: 2.5 to 17.5 ppm), except in a short interval from 1'208.5 to 1'210.5 m MD that is rich in anhydrite.
- The anhydrite layer is characterised by its high sulphur content (DWSU: up to 0.23 W/W; pure anhydrite: 0.236 W/W), low total GR (GR_KCOR: up to 8 GAPI) and high resistivities (e.g. RT_HRLT).
- Below the anhydrite layer (from 1'210.5 m and deeper), logs show relatively homogeneous values, e.g. an intermediate density-neutron separation in the limestone compatible scale, intermediate sonic (DTCO: 63 to 93 µs/ft) and homogeneous iron concentrations (DWFE: 0.02 to 0.06 W/W). These suggest intermediate to moderately high clay content as is common in marlstone.
- Matrix mineralogy indicators such as silicon (DWSI), calcium (DWCA) and the photoelectric factor (PEFZ) are variable and not consistent with clay indicators suggesting that the matrix mineralogy is mainly composed of carbonates with a siliciclastic component.

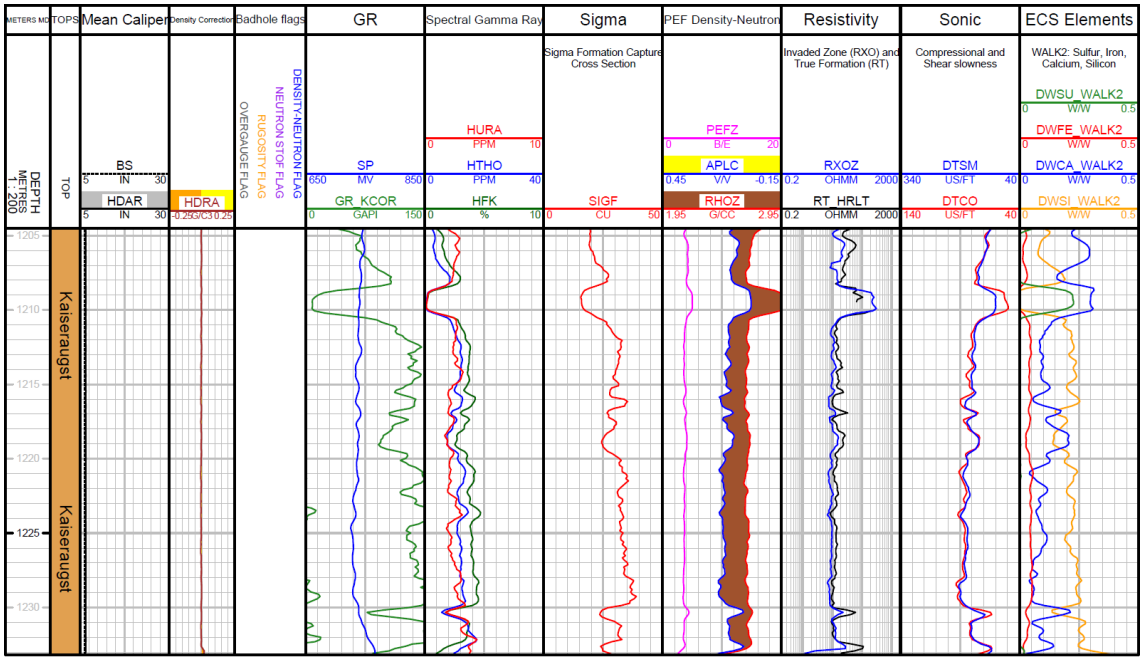

Fig. 3-11: Main logs of the composite dataset in the Kaiseraugst Formation

3.4.11 Dinkelberg Formation (1'233.2 to 1'246.1 m MD)

The top of the Dinkelberg Formation corresponds to a transition from marls to sandstones, which is represented in the logs by an increase in the silicon content (DWSI) and a decrease in calcium (DWCA), as well with a very distinctive change in the density-neutron separation, where the density log shifts to the left of the neutron log ("crossover" in a limestone-compatible scale, shaded yellow).

Logs respond well to lithology in this formation because hole conditions were good and are characterised by the following attributes (Fig. 3-11):

- Logs often show a high corrected total GR (GR_KCOR) ranging from 24 to 131 GAPI, despite the crossover in the density-neutron separation that is indicative of low clay content and mineralogy dominated by siliciclastics. This is typical for siltstones and sandstones that contain slightly radioactive minerals such as K-feldspar and mica (and are better quantified by the stochastic, multimineral analysis described in Dossier X). The relatively high potassium concentrations (HFK), ranging from 0.2 to 4.0%, also suggest the presence of radioactive minerals.
- Photoelectric factor values (PEFZ) are close to that of pure quartz (1.8 B/E), averaging at 2.1 B/E. The silicon content (DWSI) also suggest the presence of significant quartz, ranging from 0.31 to 0.47 W/W (pure quartz: 0.467 W/W).
- The large separation between the shallow (RXOZ) and deep (RT_HRLT) resistivities indicate a permeable formation that has been invaded by the mud filtrate.

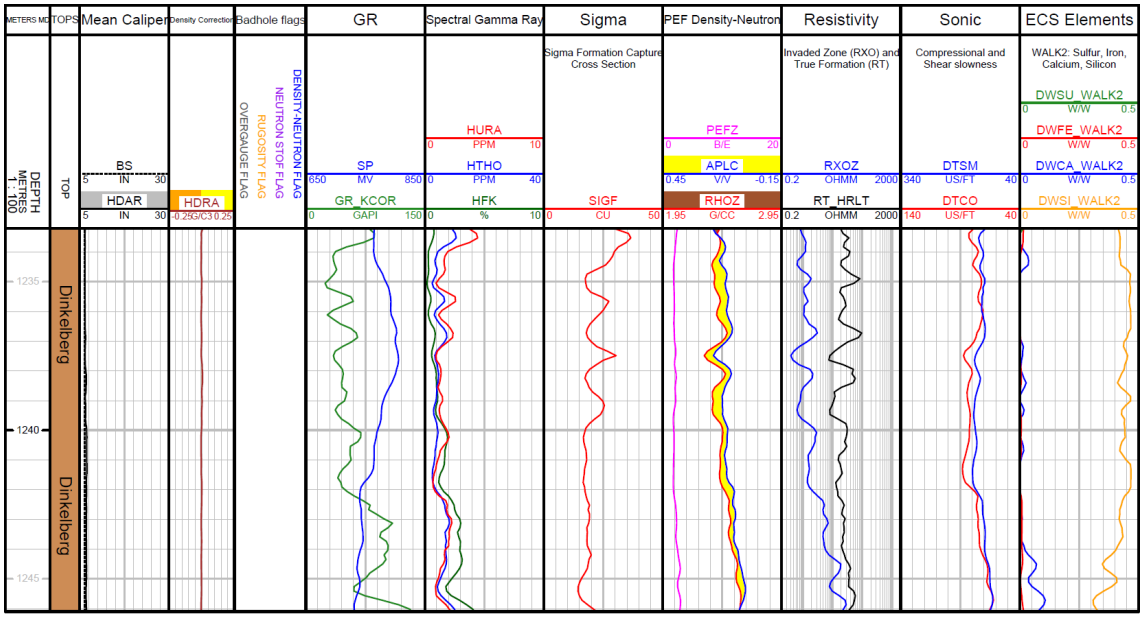

Fig. 3-12: Main logs of the composite dataset in the Dinkelberg Formation

3.4.12 Weitenau Formation (1'246.1 to 1'259.7 m MD)

The top of the Weitenau Formation is characterised by sharp increases in the clay indicators such as total GR (GR_KCOR) and sigma (SIGF).

Logs respond well to lithology in this formation because hole conditions were very good (Fig. 3-12). Logs in the Weitenau Formation have the following attributes:

- A high total GR, ranging from 117 to 150 GAPI, with a low density-neutron separation in the limestone compatible scale, indicate relatively low clay contents. This is typical for siltstones and sandstones that contain slightly radioactive minerals such as K-feldspar and mica.
- In a few zones, "crossover" is observed in the density-neutron separation (shaded yellow) indicating the presence of siliciclastic minerals such as quartz (and feldspars). This observation is supported by the high silicon content (DWSI: 0.33 to 0.41 W/W) and the low photoelectric factor (PEFZ: 2.6 to 2.9 B/E).
- Log characteristics are fairly homogeneous, which is best shown by the low variations in spectral GR contributions (potassium: HFK; thorium: HTHO; uranium: HURA).

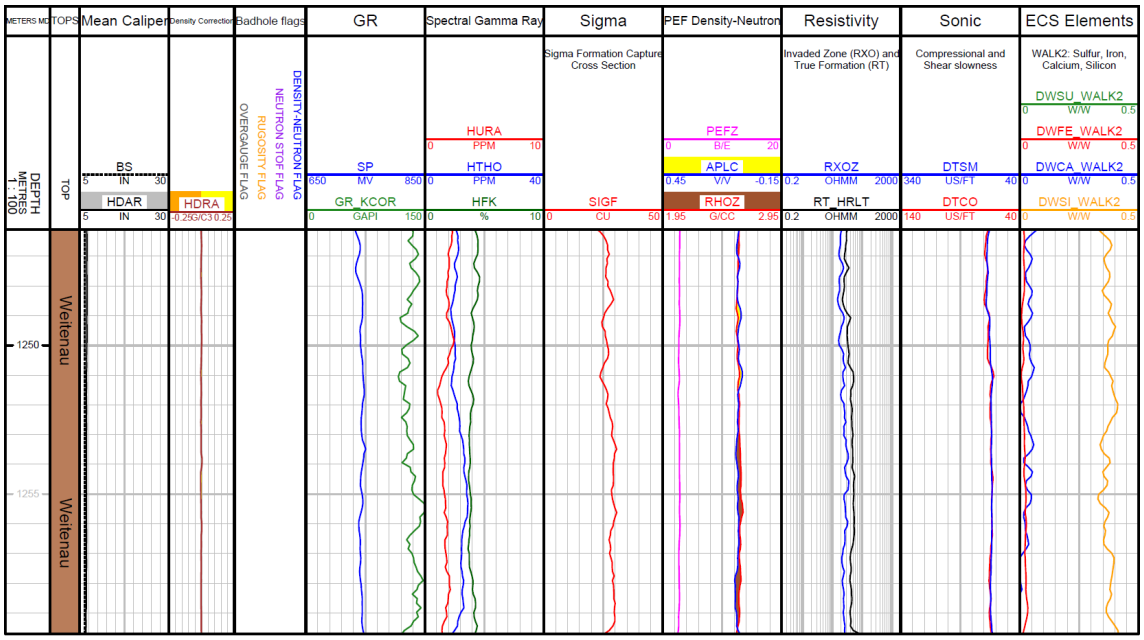

Fig. 3-13: Main logs of the composite dataset in the Weitenau Formation

3.4.13 Crystalline basement (1'259.7 m MD to borehole bottom)

The top of the crystalline basement corresponds to a "crossover" in the density-neutron separation, a slight decrease in the clay indicators (GR_KCOR; SIGF) and invasion of mud filtrate into the formation (separation of the shallow and deep resistivities: RXOZ and RT_HRLT).

Logs responded well to the lithology in this formation because hole conditions were good, except in the interval from 1'277.5 m to 1'292 m MD where the neutron log response (APLC) is degraded (see bad-hole neutron flag in Fig. 3-13). Logs have the following attributes in the crystalline basement (Fig. 3-13):

- A high and very variable total GR (GR_KOR: 95 to 343 GAPI) which is typical of crystalline metamorphic or igneous rocks that can contain slightly radioactive minerals such as K-feldspar and mica.
- In the upper part of the formation (from 1'259.7 m to 1'265.5 MD), the neutron-density "crossover" and high silicon content (DWSI: 0.36 to 0.44 W/W) indicates the presence of quartz minerals (and/or feldspars).
- Mineralogy (clays, matrix minerals) is complex and can be better quantified by the stochastic, multimineral analysis described in Dossier X.

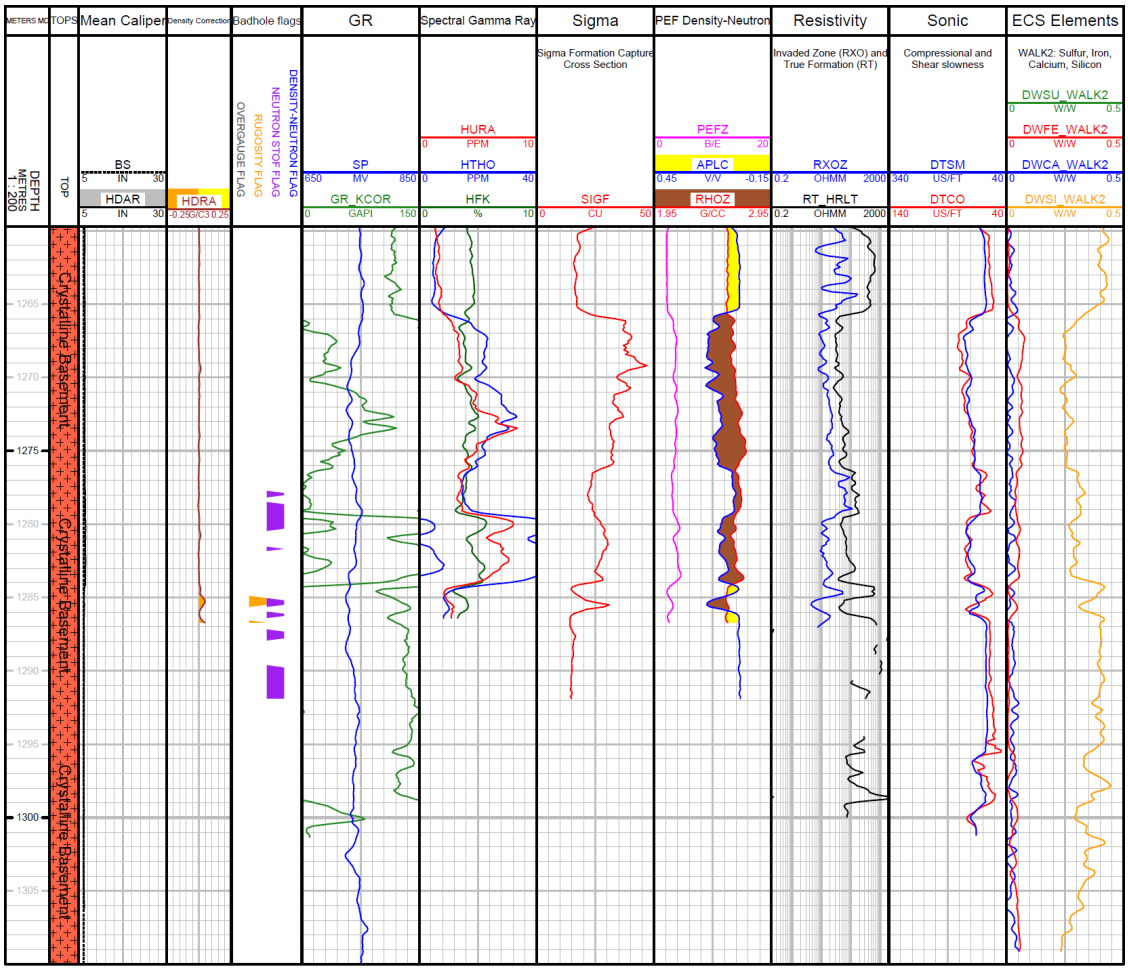

Fig. 3-14: Main logs of the composite dataset in the crystalline basement

3.5 Post-completion mud temperature

A temperature log was acquired by Schlumberger post-completion (in cased hole) on 09.04.2021 (Run 5.2.1) to measure the undisturbed temperature of the mud after the last mud circulation on 09.04.2021. Temperature was measured using the EMS tool, which has an accuracy of ± 1 °C and resolution of 0.1 °C. In Fig. 3-14, only the downlog from Run 5.2.1 is plotted as it is believed to be the most representative of the formation temperature. It was acquired at a slow rate of 193 m/hr to avoid mixing of the hydrostatic mud column. Maximum temperature of 55.36 °C was recorded at 1'131.88 m MD, minimum of 9.70 °C at surface. In Opalinus Clay, the temperature is 35.83 – 43.71 °C and the average geothermal gradient $\Delta T/\Delta D = 0.073$ °C/m (same as for Bülach1-1). The overall temperature gradient is higher in the clay-rich units of the Dogger compared to the calcareous units of Malm and Muschelkalk.

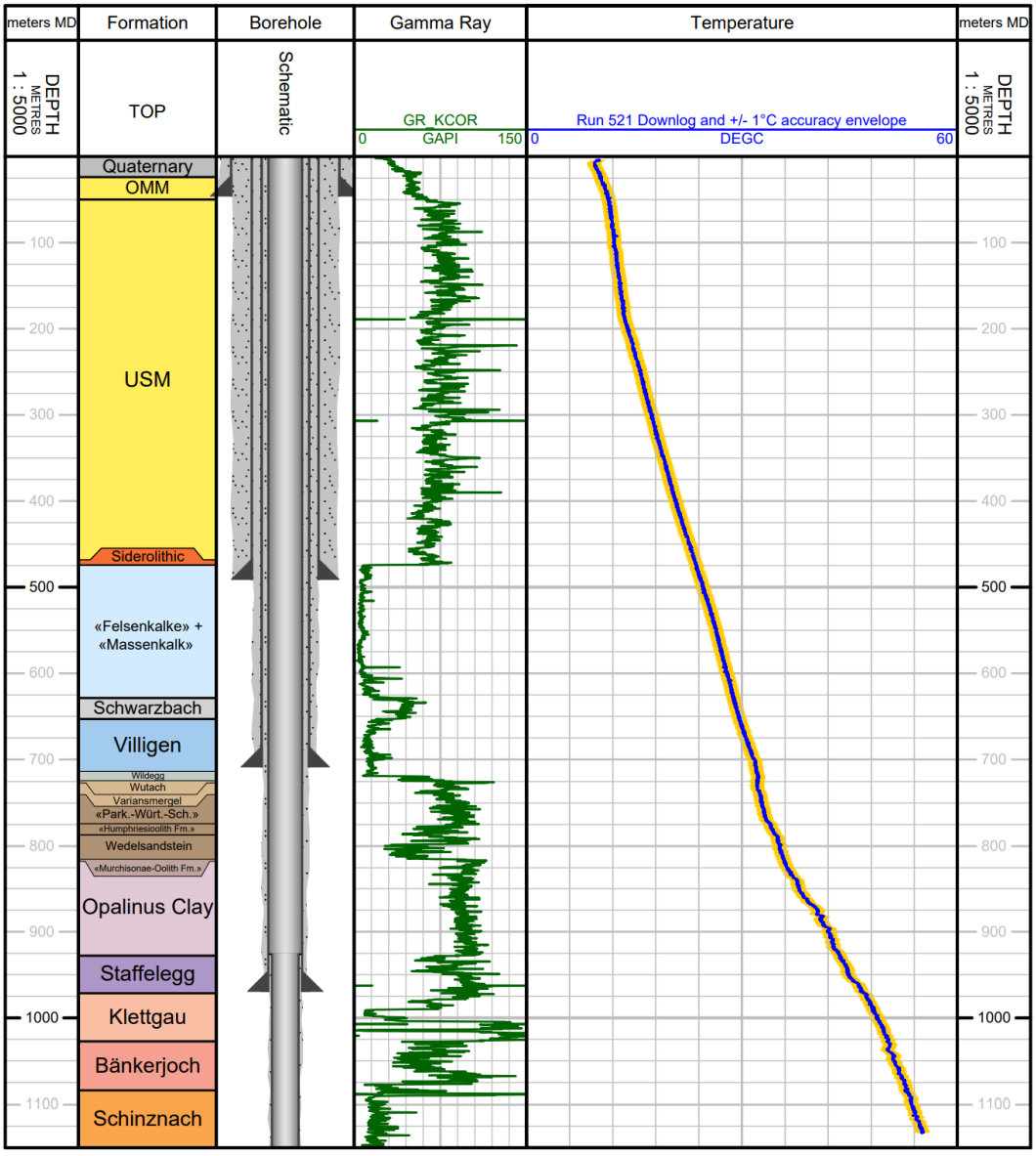

Fig. 3-15: Post-completion temperature log from the downlog pass of Run 5.2.1 (09.04.2021)
A ± 1 °C accuracy envelope is drawn in orange around the temperature log

4 Borehole Imagery (BHI)

Borehole imaging tools produce high resolution circumferential images of the borehole wall by measuring either resistivity with tool pad contact or ultrasonic velocity. For the TRU1-1 borehole, SLB's Fullbore Formation MicroImager (FMI) and Ultrasonic Borehole Imager (UBI) were used. The FMI comprises of four pads that measure the formation resistivity via an array of buttons (24 per pad) that are pressed against the borehole wall, providing a vertical resolution of 2.5 mm and 80% coverage in a 8" hole diameter. The UBI has a rotating sub that sends out acoustic pulses to the formation and measures the amplitude and travel time of the returning signals, providing 5 mm vertical resolution and 100% borehole coverage. In general, fractures, faults and bedding are more easily identifiable using the FMI than the UBI as the microresistivity images provide better contrast. However, borehole wall features can be missed if they are located in an area not covered by the tool pad, which is why FMI and UBI images should be used together for image interpretation. In addition, breakouts are typically poorly resolved on microresistivity images because fracturing and spalling associated with these breakouts result in poor contact of the tool pads with the borehole wall.

BHI was used to:

- identify and characterise geological, sedimentological and structural features including bedding, fault planes / zones and fractures
- identify stress-induced borehole phenomena such as tensile drilling-induced fractures and breakouts
- core goniometry
- select MHF testing locations (referred to as stations herein)
- detect and orient fractures induced by MHF stress measurements

For details on the first three uses of BHI, please refer to Dossier V. Only the latter two will be discussed further in the present Dossier.

The BHI, that was acquired pre-MHF, was quality-controlled (QCed), processed and interpreted by GPCI or NiMBUC in a limited amount of time (i.e. rush processing and basic quicklook interpretation). The aim of this quicklook interpretation was to provide a general and quick picture of existing borehole / rock heterogeneities (breakouts, natural and induced fractures etc.) for the selection of MHF stations immediately after BHI log acquisition and prior to MHF testing. In Fig. 4-1, the workflow used by GPCI and NiMBUC is described. Final processed and spliced pre-MHF image logs are included in the composite plots (Appendices B and C), along with the petrophysical logs and core photographs.

The post-MHF imagery underwent a similar workflow to the pre-MHF imagery, however, only the intervals that underwent stress testing were interpreted. These will be detailed in a future MHF interpretation report. To determine whether fractures were generated or enhanced (opened further), the pre- and post-MHF imagery was plotted side-by-side, along with the MHF test interval, packer positions and core photographs (see Appendix D).

Step 1: Image QC	
Depth matching	Correlate high resolution image with reference GR
Caliper check	Verify calibration with casing ID, identify if borehole conditions could affect image quality (washouts, mud cake etc.)
Hardware check	Identify if downhole equipment performance indicators such as gain and voltage supply are consistent
Orientation check	Ensure orientation data are in agreement with borehole azimuth and deviation from independent survey
Accelerometer check	Accelerometer measurement should be consistent with earth's gravity (1 g = 9.81 ± 0.03 m/s^2)
Magnetometer check	Magnetometer consistent with theoretical magnetic field strength at location, X-Y magnetometers behave complementary, QC magnetic declination parameters input
Tool movement check	Identification of any stick and pull events using tension and accelerometer measurements
Acquisition check	Verify frame time and cable speed control
Borehole image check	Identification of dead buttons or pads and any casing interference

Step 2: Image processing	
Basic image generation	Azimuthal orientation of images to true or grid north
	Merging of individual tool run passes
	Splicing of data between drilling sections
	If required, invert images to ensure per industry standards that low value = low resistivity and high value = high resistivity
	If required, correct offsets between pad images
	Bad button detection and correction
Image equalisation and normalisation	Static normalisation involving selecting the normalisation distribution (uniform/Gaussian), equalisation strength, high/low cut-offs for equalisation etc.
	Dynamic normalisation to enhance local contrasts highlighting features in a selected sliding window of a few metres

Step 3: Basic interpretation	
Manual picking of features directly from the processed image in accordance with Nagra classification scheme detailed here	Drilling-induced fractures
	Borehole breakouts
	Bedding
	Fractures (conductive, partially conductive, resistive, partially resistive, faint trace)
	Faults (conductive, partially conductive, resistive, partially resistive, faint)

Fig. 4-16: Borehole image processing workflow

5 Microhydraulic Fracturing (MHF)

5.1 Introduction and objectives

A series of stress measurements were performed in the TRU1-1 borehole using the Microhydraulic Fracturing (MHF) technique. MHF testing in boreholes is the only direct method available for measuring rock stress magnitude at great depth. An overview of the methodology can be found in Haimson (1993), Desroches & Kurkjian (1999) and Haimson & Cornet (2003) and references therein. Updates specific to this project can be found in Desroches et al. (2021). The objectives of the testing programme are to acquire data to:

- provide estimates of the in situ stress state in the Opalinus Clay and adjacent rock formations, and
- provide calibration points for mechanical earth models (MEM) of the rock mass (1D, 3D). See Bérard & Prioul (2016) for an overview of mechanical earth models and Plumb et al. (2000) for a definition of an MEM.

Key features include:

- Core images and BHI (FMI and UBI) were used to select the appropriate test depths closest to where geomechanical lab test samples were taken.
- The MHF protocol that was used, was tailored in real-time to bracket the far-field closure stress as closely as possible.
- Post-MHF imaging logs were run to determine the trace of the newly created fractures, enabling better allocation of the MHF closure stress to a principal stress direction.
- Sleeve fracturing was regularly used to focus the test on the desired interval; sleeve reopening was used to estimate the maximum horizontal stress when the MHF tests yielded an estimate of the minimum horizontal stress.

5.2 MHF theory

MHF tests an interval of approximately 1 m which is sealed above and below by packers that are approximately 0.5 m in length (exact dimensions are dependent on the configuration of the tool string). A schematic, showing the successive steps taken for a typical MHF test, is presented in Fig. 5-1. Once the interval is sealed, a microhydraulic fracturing cycle begins with pressurising the interval (1st step) until fracture initiation. Fluid keeps being injected to extend the microhydraulic fracture into the formation by a couple of decimetres (2nd step). Injection is then stopped to allow fracture closure, and pressure fall-off is observed (3rd step). Similar steps are repeated to further extend and refine the testing of the microhydraulic fracture until the test is deemed satisfactory.

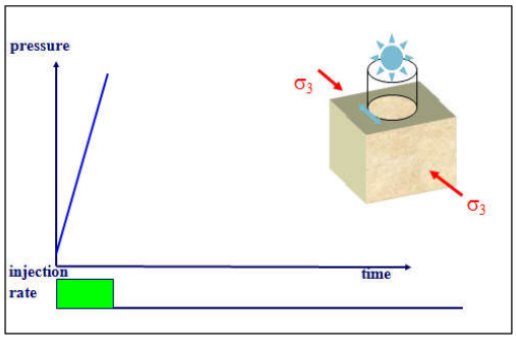

1st step: pressurisation

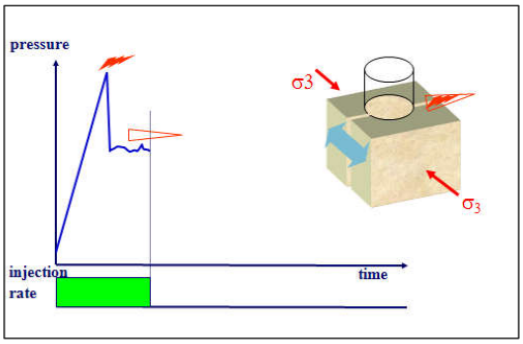

2nd step: fracture propagation

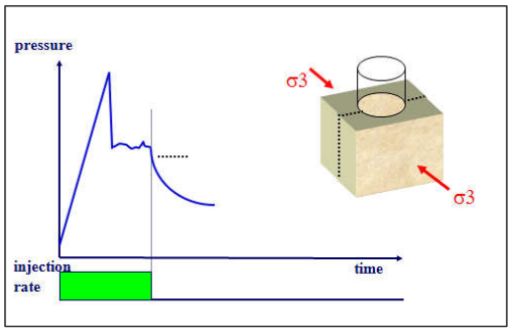

3rd step: Fracture closure

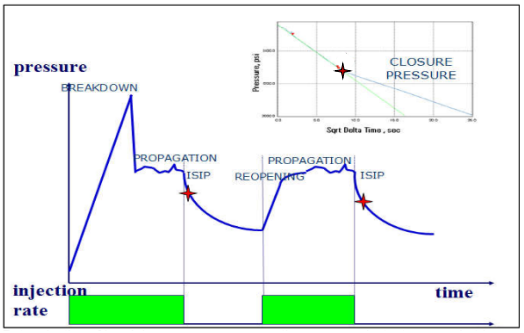

Repeat steps for subsequent cycle(s)

Fig. 5-17: Schematic showing the response of the interval pressure to fluid injection in the interval as a function of time during an MHF test and associated formation response (courtesy of SLB)

5.3 Test protocol

Each test consisted of a succession of steps according to the general test procedure described in Desroches & Kurkjian (1999), Haimson & Cornet (2003) and Wileveau et al. (2007). Although a general procedure was followed for each test, the steps were tailored in real-time to ensure that the pressure records provided the best possible estimate for closure stress (see Desroches et al. 2021). As a result, the number of steps and their nature varied from test to test.

The steps undertaken during a stress test were as follows:

- Depth correlation: validate the cable depth by comparing GR logs with the reference GR log of the borehole.
- Sleeve fracturing: this step is analogous to sleeve reopening (see below) but performed prior to the microhydraulic fracturing operation. The single packer is placed in front of the desired depth and applies pressure to focus the initiation of a longitudinal fracture at the desired interval. Note that this part of the sequence is not carried out if a pre-existing fracture (natural or drilling-induced or -enhanced) is present in the test interval.
- Packer inflation and leak-off test: the straddle packer is positioned so that the centre of the interval is in front of the desired depth. Packers are inflated to a differential pressure of 300 to 500 psi and the integrity of the seal is observed. The integrity of the seal is further validated by a short injection into the interval.

- Breakdown cycle (steps 1 to 3 in Fig. 5-1): the first cycle in a test during which a hydraulic fracture is propagated was counted as a breakdown cycle (even if technically there is no breakdown, e.g. because a pre-existing drilling-induced fracture was tested). To ensure that cycles are not counted more than once, there was only one breakdown cycle per test. Whether it starts with a step-rate test or ends with a slamback / rebound test (see below), it is still only counted as one breakdown cycle.
- Reopening cycle: any subsequent injection / shut-in cycle during which a fracture is propagated and that neither starts with a step-rate test nor ends with a slamback / rebound test (see below) is counted as a reopening cycle.
- Slamback / rebound test: at the end of an injection cycle during which a fracture was propagated (but not for the first time), the interval is quickly opened and closed for a fast depressurisation, and pressure rebounds from a value close to borehole hydrostatic pressure. The slamback occurs immediately after the injection stopped, and the rebound is observed until a plateau is reached. If the injection cycle starts with a step-rate test, it is only counted as a step-rate test and not as a slamback / rebound test.
- Step-rate test: an injection cycle during which the rate was increased (or decreased) in steps with at least three different flow rates during the cycle is called a step-rate test. An injection cycle during which the rate was only changed once cannot be counted as a step-rate test because it does not allow a step-rate interpretation.
- Sleeve reopening: the single packer is moved in front of the previously tested interval and pressure is applied with the aim of detecting and reopening the fracture created during the microhydraulic fracturing cycles.

In Fig. 5-2, an example of the pressure record for a MHF test performed in the TRU1-1 borehole is presented (Station 1-3, Run 2.1.8). The top plot (Fig. 5-2a) shows the pressure in the interval, the middle plot (Fig. 5-2b) the fluid injection rate as a function of time and the bottom plot (Fig. 5-2c), also called a reconciliation plot, the characteristic pressures estimated for all cycles for which a fracture was created / tested. For this test, there were a total of 5 MHF cycles, labeled 5 to 11. The first cycles are not analysed as they correspond to the packer inflation and leak-off test. Cycle 5 corresponds to the breakdown and propagation cycle, similar to what was depicted in the theory schematic (Fig. 5-1). Cycles 6 and 9 are reopening tests, cycles 7 and 11 are step-rate tests. A slamback / rebound test was performed at the end of cycles 7 and 11. The characteristic pressures presented in the bottom plot reflect the stress acting on the fracture: they validate the creation of a hydraulic fracture and show a clear trend towards convergence that supports that an estimate of the far-field stress can be obtained from the test.

The raw MHF pressure-time and reconciliation plots for all tests conducted in the TRU1-1 borehole are included in Appendix E. In Tab. 5-1, a summary step taken for each MHF station is given, along with the associated formation / unit that was tested. Stations are presented in operational order.

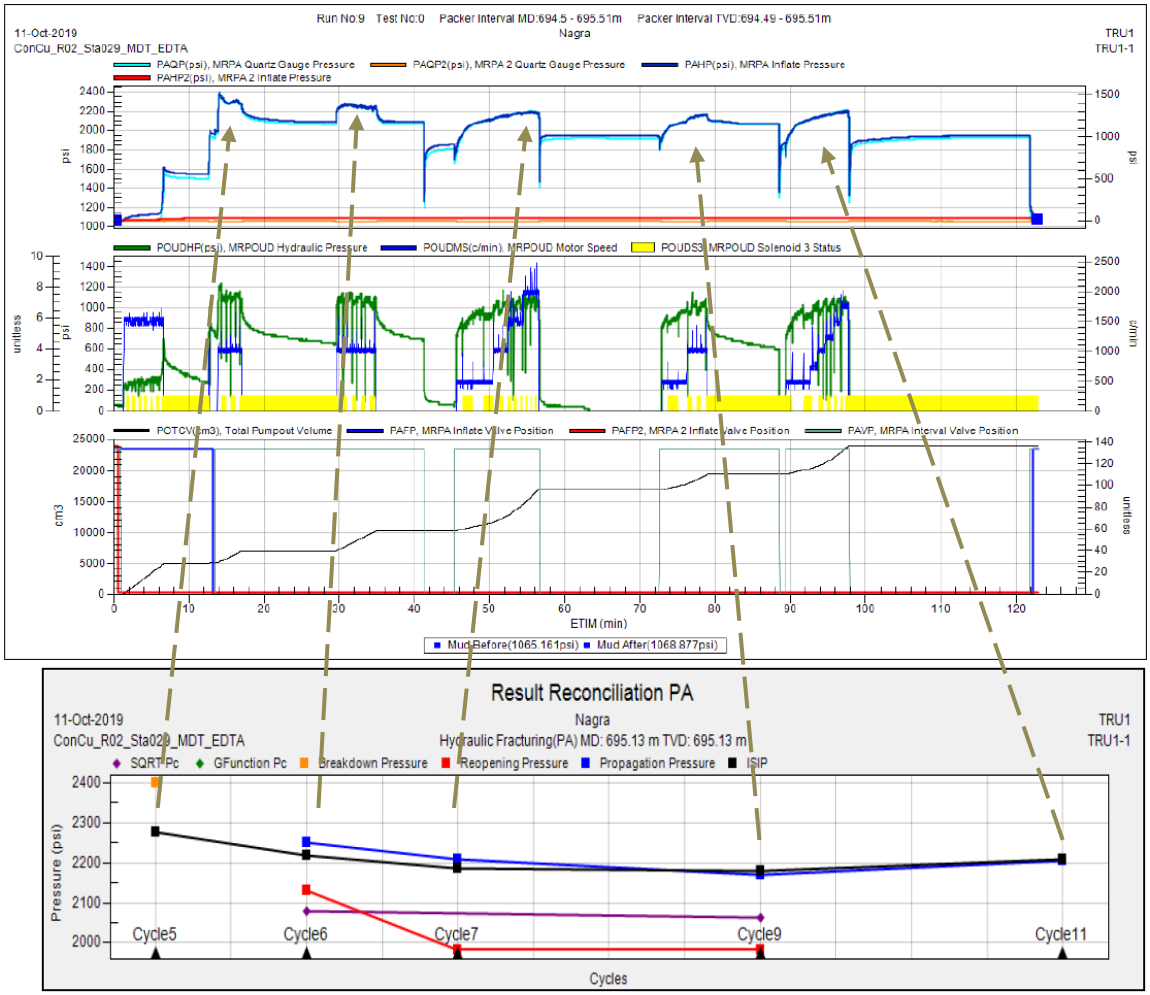

Fig. 5-18: Example of pressure record for MHF test from TRU1-1 (Station 1-3, Run 2.1.8)
Pc stands for closure pressure, ISIP stands for Instantaneous Shut-in Pressure.

Tab. 5-7: Summary of MHF station locations and operations carried out for each phase of the TRU1-1 borehole

Phase / Section	**Station**	**Formation / unit**	**Middle interval depth** [m]	**Sleeve fracturing cycles**	**Breakdown cycles**	**Reopening cycles**	**Slamback / rebound tests**	**Step-rate tests**	**Sleeve reopening cycles**
II (Run 2.1.8)	1-2	Villigen Fm.	697.8	No	1	4	0	1	2
	1-3	Villigen Fm	695.0	2	1	2	0	2	2
	2-1	Schwarzbach Fm.	633.25	2	0	0	0	0	No
	2-2	Schwarzbach Fm.	644.7	2	1	2	1	1	2
	2-4	Villigen Fm.	653.8	No	1	1	0	3	2
	3-1	«Felsenkalke» + «Massenkalk»	606.6	2	1	2	0	2	2
	3-3	«Felsenkalke» + «Massenkalk»	515.15	2	1	4	1	1	2
III (Run 3.4.3)	1-1	«Parkinsoni-Württembergica-Schichten»	757.35	2	1	1	1	2	2
	2-1	Wedelsandstein Fm.	789.2	2	1	3	0	2	2
	3-1	Opalinus Clay	841	2	1	2	1	3	2
	3-2	Opalinus Clay	843.6	No	1	2	0	3	No
	3-3	Opalinus Clay	916.25	2	1	2	0	2	2
	3-4	Opalinus Clay	856.45	2	1	1	0	4	2
	3-6	Opalinus Clay	819.4	2	1	2	0	3	2
	4-2	Wildegg Fm.	724.25	No	1	3	1	2	2

Tab. 5-1: continued

Phase / Section	**Station**	**Formation / unit**	**Middle interval depth** [m]	**Sleeve fracturing cycles**	**Breakdown cycles**	**Reopening cycles**	**Slamback / rebound tests**	**Step-rate tests**	**Sleeve reopening cycles**
IV (Run 4.4.2)	1-2	Schinznach Fm.	1'093.1	1	1	2	1	1	3
	2-1	Klettgau Fm.	989.8	2	1	1	2	1	2
	2-2	Klettgau Fm.	1'026.5	2	1	0	2	2	No
IV (Run 4.5.2)	3-2	Bänkerjoch Fm.	1'051.55	2	1	1	2	2	2
	3-3	Bänkerjoch Fm.	1'076.2	No	1	0	1	3	2
	3-4	Bänkerjoch Fm.	1'053.6	2	1	3	0	2	2
	4-1	Schinznach Fm.	1'097.32	2	1	2	1	3	2
V (Run 5.1.7)	1-1	Zeglingen Fm.	1'170.1	2	0	0	0	0	No
	1-2	Zeglingen Fm.	1'192.0	No	0	0	0	0	2
	1-3	Zeglingen Fm.	1'165.2	No	0	0	0	0	No
	1-4	Zeglingen Fm.	1'196.0	2	0	0	0	0	No
	2-1	Dinkelberg Fm.	1'243.65	No	1	4	1	1	2
	2-2	Weitenau Fm.	1'248.2	No	0	0	0	0	No

5.4 MHF results

28 tests were attempted, with 22 of them being successful, from the «Felsenkalke» + «Massenkalk» unit (474 m) down to the Weitenau Formation (1'260 m). Tests without the ability to breakdown the formation or with an inability to maintain a high-pressure seal were deemed unsuccessful. Any other test where a closure stress could be estimated was deemed successful.

Tab. 5-2 presents a quicklook interpretation of the MHF results which includes the 'breakdown pressure', the closure stress range and associated comments. The 'breakdown pressure' is taken as the maximum pressure reached during the first hydraulic fracturing cycle. A classical breakdown pressure interpretation should not be applied to these pressure values because sleeve fracturing was performed prior to hydraulic fracturing. Recorded 'breakdown pressures' are therefore technically reopening pressures. The closure stress acts normal to the fracture surface. Its range was determined from the pressure records and expressed with a lower and an upper bound.

Fig. 5-3 plots the closure stress ranges from the quicklook analysis as a function of depth together with the overburden vertical stress (Sv), estimated from integration of the density logs over depth, and the maximum pressures measured during the formation integrity tests (FIT).

Quicklook analysis of the post-MHF borehole imagery showed that new or enhanced features (longitudinal) could be observed at successful station locations. Conversely, in unsuccessful tests, no new feature could be observed. Fig. 5-4 presents the pre- and post-MHF images for Station 1-3 (Run 2.1.8). New fracture traces induced by the MHF test are shown with blue arrows on the rightmost track. A comparison of all the pre- and post-MHF borehole images is included in Appendix D.

Interpretation of sleeve fracturing / sleeve reopening tests was not performed as part of the acquisition programme and is not included in this report.

Tab. 5-8: Quicklook interpretation of MHF results for the TRU1-1 borehole

Section Run Diameter	**Station**	**Formation**	**Depth** [m]	**Breakdown pressure** [MPa]	**Closure stress range** [MPa]	**Comments**
II Run 2.1.8 6 ⅜" bit size	3-3	«Felsenkalke» + «Massenkalk»	515.15	17.14	10.0 – 11.9	Shmin likely
	3-1	«Felsenkalke» + «Massenkalk»	606.6	15.21	12.4 – 13.8	Shmin likely
	2-1	Schwarzbach Fm.	633.25	> 41.35 *	N/A	No breakdown acheived
	2-2	Schwarzbach Fm.	644.7	12.66	9.7 – 11.9	Shmin likely
	2-4	Villigen Fm.	653.8	12.78	11.3 – 12.8	Shmin or Sv?
	1-3	Villigen Fm.	695	16.54	13.4 – 15.2	Shmin or Sv?
	1-2	Villigen Fm.	697.8	12.71	12.1 – 14.2	Erratic closure behaviour
III Run 3.4.3 6 ⅜" bit size	4-2	Wildegg Fm.	724.25	15.20	13.5 – 14.5	Shmin likely
	1-1	«Parkinsoni-Württembergica-Schichten»	757.35	16.93	11.1 – 16.4	Shmin likely
	2-1	Wedelsandstein Fm.	789.2	17.28	15.1 – 15.9	Shmin likely
	3-6	Opalinus Clay	819.4	18.63	14.2 – 17.9	Shmin likely
	3-1	Opalinus Clay	841	19.21	15.0 – 17.3	Shmin likely
	3-2	Opalinus Clay	843.6	20.18	16.8 – 19.3	HTPF test: upper bound for Shmin
	3-4	Opalinus Clay	856.45	19.39	16.0 – 17.8	Shmin likely
	3-3	Opalinus Clay	916.25	17.43	11.6 – 15.9	Unknown
IV Runs 4.4.2 & 4.5.2 8 ½" bit size	2-1	Klettgau Fm.	989.8	22.67	20.0 – 22.0	Shmin likely
	2-2	Klettgau Fm.	1'026.5	22.70	19.3 – 22.1	Shmin likely
	3-2	Bänkerjoch Fm.	1'051.55	28.51	23.4 – 25.5	Shmin or Sv?
	3-4	Bänkerjoch Fm.	1'053.6	26.39	21.3 – 24.7	Shmin or Sv?
	3-3	Bänkerjoch Fm.	1'076.2	30.6	25.5 – 29.7	Unknown
	1-2	Schinznach Fm.	1'093.1	25.26	13.8 – 19.3	Shmin likely
	4-1	Schinznach Fm.	1'097.32	29.5	13.2 – 19.3	Shmin likely
V Run 5.1.7 6 ⅜" bit size	1-3	Zeglingen Fm.	1'165.2	> 44.88 *	N/A	No breakdown achieved. Extremely high effective tensile strength of the rock?
	1-1	Zeglingen Fm.	1'170.1	> 26.01 *	N/A	
	1-2	Zeglingen Fm.	1'192	> 39.85 *	N/A	
	1-4	Zeglingen Fm.	1'196	> 38.69 *	N/A	
	2-1	Dinkelberg Fm.	1'243.65	40.34	26.1 – 30.0	Shmin likely
	2-2	Weitenau Fm.	1'248.2	> 42.68 *	N/A	No breakdown achieved
Total number of tests						28
Total number of successful tests						22
Success rate (actual vs. attempted) & (actual vs. desired from initial plan)						79% & 110%

* If no hydraulic fracture could be created, the maximum pressure applied to the interval was provided.

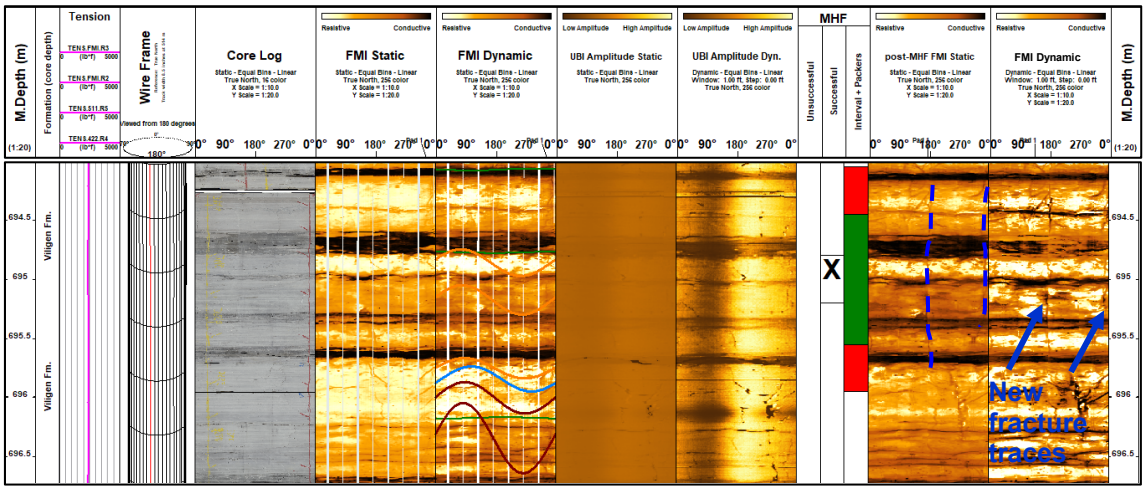

Fig. 5-19: Example of pre- vs. post-MHF images from TRU1-1 (Station 1-3, Section II)

Pre- and post-MHF images are presented on the left and right of the MHF columns, respectively.

New fracture traces are highlighted with dashed blue lines on the FMI static image and with arrows on the FMI dynamic image.

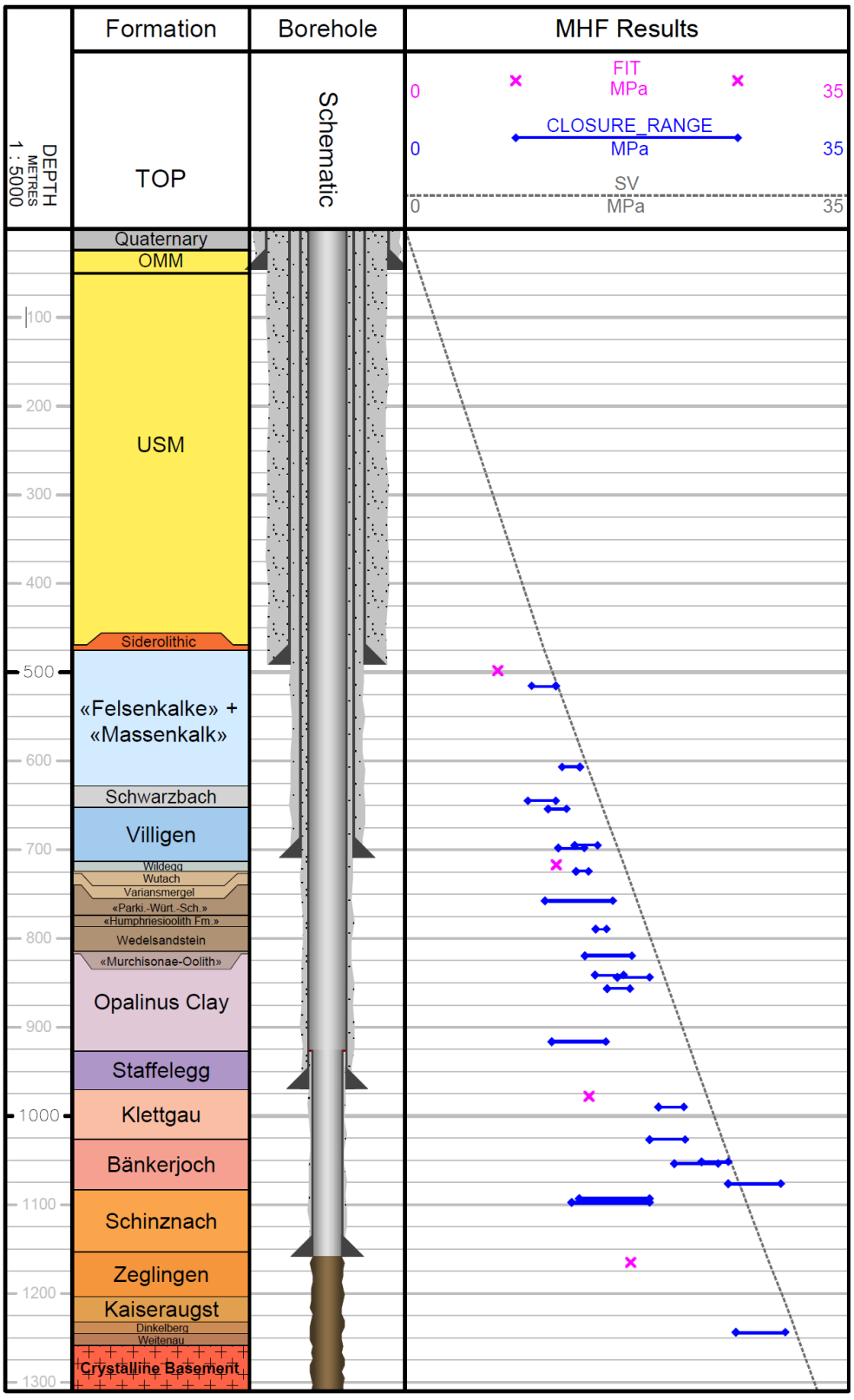

Fig. 5-20: Comparison of the quicklook closure stress range obtained from the TRU1-1 MHF tests with the overburden vertical stress (Sv) from the integration of density over depth and the maximum pressures attained during the formation integrity tests (FIT)

6 References

Bérard, T. & Prioul, R. (2016): Mechanical Earth Model. Oilfield Review: The Defining Series, https://www.slb.com/resource-library/oilfield-review/defining-series/defining-mem.

Desroches, J. & Kurkjian, A.L. (1999): Applications of wireline stress measurements. Paper SPE-58086, SPE Reservoir Evaluation & Engineering 2/5, 451-461. DOI:10.2118/ 58086-PA.

Desroches, J., Peyret, E., Gisolf, A. Wilcox, A., Di Giovanni, M., Schram de Jong, A., Sepehri, S., Garrard, R. & Giger, S. (2021): Stress measurement campaign in scientific deep boreholes: Focus on tool and methods. SPWLA Paper #2021-056 presented at the SPWLA 62nd Annual Logging Symposium, May 17-20 2021.

Haimson, B.C. (1993): The Hydraulic Fracturing Method of Stress Measurement: Theory and Practice. Chapter 14 *in:* Hudson, J. (ed.): Comprehensive Rock Engineering 3, 395-412, Pergamon Press. DOI: 10.1016/B978-0-08-042066-0.500215.

Haimson, B.C. & Cornet, F.H. (2003): ISRM suggested methods for rock stress estimation – Part 3: Hydraulic Fracturing (HF) and/or Hydraulic Testing of Pre-Existing Fractures (HTPF). International Journal Rock Mechanics and Mining Sciences 40/7-8, 1011-1020. DOI: 10.1016/j.ijrmms.2003.08.002.

Isler, A., Pasquier, F. & Huber, M. (1984): Geologische Karte der zentralen Nordschweiz 1:100'000. Herausgegeben von der Nagra und der Schweiz. Geol. Komm.

Nagra (2014): SGT Etappe 2: Vorschlag weiter zu untersuchender geologischer Standortgebiete mit zugehörigen Standortarealen für die Oberflächenanlage. Geologische Grundlagen. Dossier II: Sedimentologische und tektonische Verhältnisse. Nagra Technischer Bericht NTB 14-02.

Pietsch, J. & Jordan, P. (2014): Digitales Höhenmodell Basis Quartär der Nordschweiz – Version 2013 (SGT E2) und ausgewählte Auswertungen. Nagra Arbeitsbericht NAB 14-02.

Plumb, R., Edwards, S., Pidcock, G., Lee, D. & Stacey, B. (2000): The Mechanical Earth Model concept and its application to high-risk well construction projects. SPE Paper #59128 presented at the IADC/SPE Drilling Conference, New Orleans, Louisiana, February 2000. DOI: https://doi.org/10.2118/59128-MS.

Schlumberger (2013): Log Interpretation Charts. https://www.slb.com/resource-library/book/log-interpretation-charts.

Serra, O. (1984): Fundamentals of well-log interpretation. Developments in Petroleum Science 15A. ELSEVIER Amsterdam, Oxford, New York & ELF AQUITAINE, Pau.

Wileveau, Y., Cornet, F.H., Desroches, J. & Blumling, P. (2007): Complete in situ stress determination in an argillite sedimentary formation. Physics and Chemistry of the Earth Parts A/B/C 32/8-14, 866-878. DOI: 10.1016/j.pce.2006.03.018.